Palacký University Olomouc
Faculty of Science
Laboratory of Growth Regulators

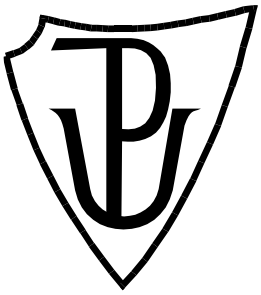

Effect of astrocytes and glial cells on tau-protein seeding in 2D and 3D cultures

Master Thesis

Author: **Ihor Kozlov**
Study program: B1501 Experimental Biology
Field of study: Experimental Biology
Form of study: Full-time
Supervisor: **Mgr. Viswanath Das, Ph.D.**

Olomouc 2023

Bibliographical identification:

Author's first name and surname:	Ihor Kozlov
Title:	Effect of astrocytes and glial cells on tau-protein seeding in 2D and 3D cultures:
Type of thesis:	Master
Department:	Laboratory of Growth Regulators
Supervisor:	Mgr. Viswanath Das, Ph.D.
The year of presentation:	2023
Keywords:	Tau aggregates, Alzheimer's disease, spheroids, tauopathy, tau seeding
Number of pages:	67
Language:	English

Summary:

Due to the growing number of patients with various forms of dementia associated with tau pathologies, choosing a reliable model for studying the mechanisms of tau sorting, seeding and the formation of pathological protein aggregates is essential. Therefore, developing trustworthy tauopathy *in vitro* models is crucial for further fundamental and pharmacological research. The conditions for cultivating the neuroblastoma cell line were compared in the thesis, and the possibility of performing the tau seeding assays in two-dimensional and three-dimensional versions was explored. It was shown that SH-SY5Y differentiated with RA and BDNF are suitable for research of TAU sorting and seeding with R3 aggregates. Differentiated cells also showed a significant increase in the production of Choline Acetyltransferase, which indicates the direction of their development in favor of cholinergic neurons.

A cell line miming astrocytes (SNB-75) was chosen due to the expression of the glial fibrillary acidic protein. It can be cultured simultaneously with SH-SY5Y. The protocol for their differentiation in co-culture was also established. SNB-75 cells demonstrated the ability to influence tau seeding. The seeding activities in mono- and co-cultures were observed using fluorescent microscopy. The differentiation was controlled by morphology analysis and western blotting. The cell lines are characterized by a comparatively low cost of cultivation, the ease of genetic modification, the possibility of differentiation and the formation of spheroids. They may be of interest as a basis for creating a three-dimensional model of the co-culture of cells with the properties of astrocytes and neurons, which can reflect the conditions for the initial stage of tauopathy with a minimum of time and financial resources spent.

Bibliografická identifikace:

Jméno a příjmení autora:	Ihor Kozlov
Název práce:	Vliv astrocytů a gliových buněk na výsev tau-proteinu ve 2D a 3D kulturách.:
Typ práce:	Diplomová
Pracoviště:	Laboratoř růstových regulátorů
Vedoucí práce:	Mgr. Viswanath Das, Ph.D.
Rok obhajoby práce:	2023
Klíčová slova:	Tau agregáty, Alzheimerova choroba, sféroidy, tauopatie, tau seeding
Počet stran:	67
Jazyk:	Angličtina

Souhrn:

Vzhledem k rostoucímu počtu pacientů s různými formami demence spojenými s patologií tau je zásadní zvolit spolehlivý model pro studium mechanismů třídění, výsevu a tvorby patologických proteinových agregátů tau. Vývoj důvěryhodných modelů tauopatie in vitro je proto zásadní pro další základní a farmakologický výzkum. V práci byly porovnány podmínky kultivace neuroblastomové buněčné linie a byla prozkoumána možnost provádění testů tau výsevu ve dvojrozměrné a trojrozměrné buněčné kultuře. Ukázalo se, že SH-SY5Y diferencované pomocí RA a BDNF jsou vhodné pro výzkum třídění TAU a výsevu R3 agregátů. Diferencované buňky také vykazovaly významné zvýšení produkce cholin acetyltransferázy, což naznačuje směr jejich vývoje ve prospěch cholinergních neuronů.

Buněčná linie napodobující astrocyty (SNB-75) byla vybrána kvůli expresi gliálního fibrilárního kyselého proteinu. Bylo prokázáno, že ji můžeme kultivovat současně s SH-SY5Y. Byl rovněž stanoven protokol pro jejich diferenciaci ve společné kultuře. Buňky SNB-75 prokázaly schopnost ovlivňovat výsev tau. Aktivita výsevu v monokultuře a v kokultuře byla pozorována pomocí fluorescenční mikroskopie. Diferenciace byla kontrolována morfologickou analýzou a western blottingem. Buněčné linie se vyznačují relativně nízkými náklady na kultivaci, snadnou genetickou modifikací, možností diferenciace a tvorby sféroidů. Mohou být zajímavé jako základ pro vytvoření trojrozměrného modelu společné kultivace buněk s vlastnostmi astrocytů a neuronů, který může odrážet podmínky počátečního stadia tauopatie s minimem vynaložených časových a finančních prostředků.

“I declare that this Master Thesis was developed independently, under the guidance of my supervisor, and by using the cited literature.”

In Olomouc, ……..…… Signature …….……..

ACKNOWLEDGMENT

This Master's thesis was performed at the Institute of Molecular and Translational Medicine in collaboration with Palacký University in Olomouc.

I would like to express my heartfelt gratitude to my supervisor, Mgr. Viswanath Das, Ph.D., for his friendliness and patience with me, an indication of my mistakes while planning experiments and advice in reading the literature to expand my theoretical scientific horizons. I would like to express my special thanks to Mgr. Narendran Annadurai for his help demonstrating the principles of operation and protocols for maintaining instruments in the institute's laboratories, finding the chemicals and moral support. Both taught me new skills for implementing this scientific work and will be important in my future career. I would also like to thank Mgr. Anna Janoštáková and Bc. Renata Buriánová for their help; their advice and support in the laboratory were priceless.

This work was supported in parts by infrastructural projects (CZ-OPENSCREEN – LM2023052; EATRIS-CZ – LM2023053), the European Regional Development Fund (ENOCH, CZ.02.1.01/0.0/0.0/16_019/0000868), the project National Institute for Neurological Research (Program EXCELES, ID Project No. LX22NPO5107) - Funded by the European Union - Next Generation EU from the Ministry of Education, Youth and Sports of the Czech Republic (MEYS), and the Grant Agency of the Czech Republic (23-06301J).

TABLE OF CONTENTS

List of Figures

List of Tables

List of Abbreviations

AD – Alzheimer's Disease

APS – Ammonium Persulphate

BDNF – Brain-Derived Neurotrophic Factor

BSA – Bovine Serum Albumin

ChAT – Choline Acetyltransferase

DMEM – Dulbecco's Modified Eagle Medium

DMSO – Dimethyl Sulfoxide

DSA – Donkey Serum Albumin

FCS – Fetal Calf Serum

GFAP – Glial Fibrillary Acidic Protein

GFP – Green Fluorescent Protein

GSA – Goat Serum Albumin

IBMX – 3-isobutyl-1-methylxanthine

MAP2 – Microtubule-Associated Protein 2

NBM – Neurobasal Medium

PD – Parkinson's Disease

PK – Protein Kinase

R2, R3 – Repeat 2, Repeat 3

RA – Retinoic Acid

Sph – Synaptophysin

TAU (tau) – Tubulin Associated Unit

Tetramethylethylenediamine – TEMED

TH – Tyrosine Hydroxylase

VGLUT1 – Vesicular Glutamate Transporter 1

1 INTRODUCTION

According to the Alzheimer Europe organization, 6,650,228 women and 3,130,449 men are affected by dementia in Europe. According to data published in 2018, 149,633 cases were recorded in the Czech Republic, approximately 1.41% of the entire population. According to forecasts, in 2050, this number may already be up to 2.65% while maintaining the trend of increasing life expectancy and low effectiveness of treatment with cholinesterase inhibitors and NMDA receptor antagonists (Georges et al., 2020). Tauopathies are characterized by tau deposits in the brain (including neurons, glia and extracellular fluid), with symptoms of dementia and parkinsonism (including cognitive/behavioral disorders, language disorders, movement disorders, and the inability to do daily activities). Diseases differ both in the mechanism of development and symptoms. For example, memory loss is a more prominent symptom in early Alzheimer's Disease (AD), but blood pressure drops on standing, falls, and urinary incontinence are common signs in dementia with Lewy bodies. Due to an increase in the number of people suffering from aging-associated diseases characterized by the accumulation of intracytoplasmic aggregates of Tubulin Associated Unit (tau) protein, there is a growing demand for creating cellular models for studying the mechanisms of pathological processes and drug testing.

Tau seeding is a characteristic phenomenon that begins well before the development of grey matter atrophy in the brains of patients diagnosed with tauopathies, such as AD, frontotemporal dementia, Parkinson's Disease (PD), progressive supranuclear palsy and corticobasal degeneration. Seeding is the ability of tau as aggregates to recruit naive tau monomers or particles of functional fibrils and fold into pathological 3D forms (Furman et al., 2017). Analysis of the literature has shown that traditional cell models give uncertain results since the conditions for cultivating cells in these systems directly contradict physiological conditions. The complexity of the interactions between neurons, astrocytes and other brain cells in a living organism is undeniable. This thesis will focus on developing 2D and 3D co-cultures of neuronal and non-neuronal cell lines to mimic brain physiology in a dish better and studying the mechanism of tau seeding in the developed systems.

2.1 AIM OF THE THESIS

The aim of this master thesis is to create cellular models of neuronal monoculture and co-culture of neuron-like cells with glial cells for studying the mechanisms of TAU seeding capable of reflecting human brain tissue properties in tauopathies and compare its characteristics in 3D and 2D.

2.2 OBJECTIVES

The main objectives of this work were to lay the foundation for the formation of a cellular model on which tau seeding can be further investigated to model AD and other tauopathies with further drug testing.

1) Find the conditions for differentiation of cells with the characteristics of mature cholinergic neurons (morphological and biochemical).

2) Find the conditions for the formation of cells with the characteristics of astrocytes (morphological and biochemical).

3) Determine the conditions under which cells mimicking mature neurons and astrocytes will exist in co-culture and under which it will be possible to test hypotheses about the mechanisms of the spread of pathological tau (seeds).

4) Recreate or modify the above conditions for cultures of spheroids.

3. LITERATURE REVIEW

3.1 Tau in Health and Disease

3.1.1 Tau Genetics and Structure

The location of the MAPT gene was first determined using the hybridization method on chromosome 17 by hybridization of a cDNA clone (Neve et al., 1986). In adult humans, at least 6 isoforms are formed by alternative splicing of the MAPT gene. The length of the protein may vary from 352 to 441 amino acid residues. The nucleotide sequence in exons 0 and 14 and part of exons 1 and 13 do not carry information that will be translated. Exon 2 incorporation is regulated during human development. It is excised during embryonic development and observed again during tissue differentiation, but only in the CNS. Information from exon 3 is present in the amino acid sequence only if exon 2 also occurs in the mature mRNA. The mechanism of inclusion of the longest exon 4A, which is relevant for the peripheral nervous system, is not fully known. Interest in studying alternative splicing of exon 10 is associated with the relationship between the ratio of isoforms with and without it and CNS pathologies in humans (Ruiz-Gabarre et al., 2022). Two haplotypes of the MAPT gene, H1 and H2, differ in the inverted or not gene sequence. The inversion and variable number of low-copy repeats are more common in Europeans and rarely found in native African populations. Recombination between low-copy repeats can potentially cause microdeletion in people with learning disabilities (Caffrey and Wade-Martins, 2007).

At least 112 mutations are known, but the relationship with diseases for 40 has not been found. There are 15 tau mutations correlated with AD, but most of them are benign. MAPT mutations, such as P301L and P301L, used in experimental models of tauopathy, play an important role in tau spreading. Alternative splicing products are isoforms coded as 0N3R, 1N3R, 2N3R, 0N4R, 1N4R and the longest present in humans - 2N4R. The first number corresponds to the number of repeats in the N-terminal domain the second one reflects the number of repeats in the Microtubule-Binding Domain (Heinisch and Brandt, 2016). Others are connected to corticobasal degeneration, progressive supranuclear palsy, PD and Pick's disease. Mutations in exon 10 can alter splicing, leading to an imbalance in the distribution of 3R and 4R tau isoforms in the brain (Chu and Liu, 2019; Strang et al., 2018). It should not be forgotten that imbalance is an essential but not necessary factor for the onset of neurodegeneration due to tau pathology. The 4R to 3R tau isoforms ratio is approximately 1 in the normal adult brain. However, this ratio is differentially altered in tauopathies, resulting in an imbalance in 4R to 3R isoforms, regardless of whether the ratio shifts in favor of 4R or 3R. In most AD cases, this ratio stays 1:1. Examples of isoform imbalance are shown in the table below:

Table 3.1: 3R/4R tau ratios in tauopathies (according to Fuster-Matanzo et al., 2018).

Tauopathies	Tau 3R/4R Ratio
Primary Tauopathies	
Richardson's syndrome	1:2–4
Pick's disease	3:1
Frontotemporal dementia with Parkinsonism	1:2
Postencephalic PD	1:1
Argylophilic grain disease	1:2
Corticobasal degeneration	1:2
Progressive supranuclear palsy	1:3–4
Parkinson-dementia complex	1:1
Secondary Tauopathies	
AD	1:1
Down's syndrome	1:1
Dementia pugilistica	1:1

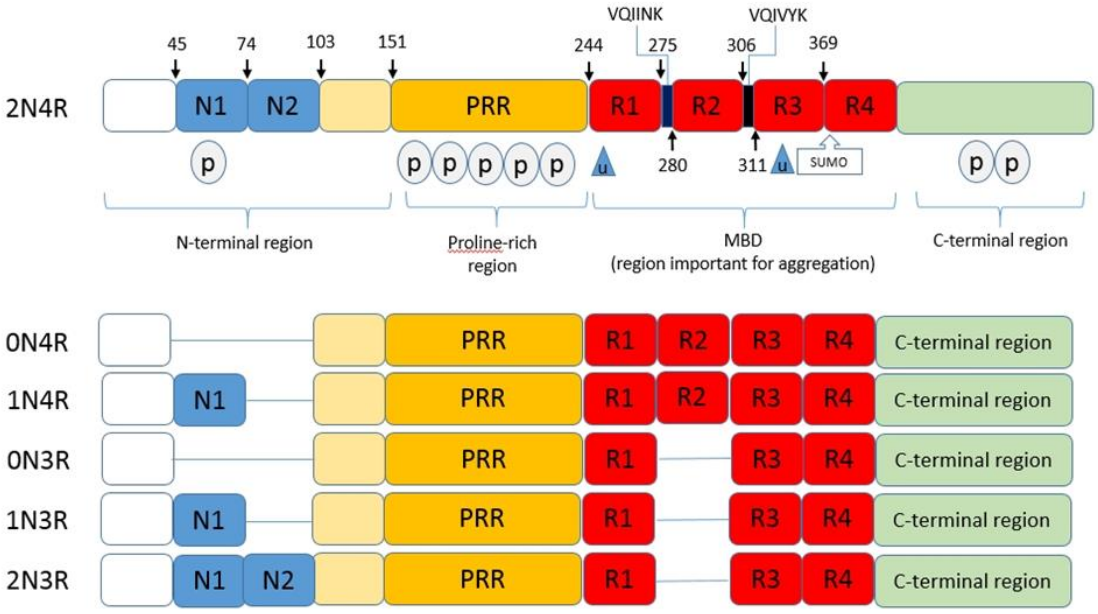

Figure 3.1: Tau isoforms with domain structures and modifications localizations: phosphorylation (P), ubiquitination (U) and SUMOylation (SUMO). Phosphorylation modifications are shown relative to the frequency of their occurrence.

Table 3.2 MAPT mutations connected with tauopathies (compiled and modified according to (Cruts et al., 2012; Karch et al., 2019).

Mutation	Associated Disease	Connection with Repetitions	Cell Types Involved	Phenotypic Manifestation
Chr17:'44087780 C>T	Frontotemporal dementia	4R isoforms of tau	Neurons, glia	An increase in exon 10 inclusion frequency; An increased proportion of 4R isoforms of tau.
Chr17:44039717 G>T	Supranuclear palsy	0N4R,1N3R,1N4R	Neurons, glia	Insoluble tau in cortical regions. Loss of the ability of tau to promote microtubule assembly.
Chr17:44049254 G>A (G55R)	Frontotemporal dementia	4R isoforms of tau	Neurons	Frontal and temporal atrophy. Tau with this mutation in 4R performs microtubule assembly more effectively than the naïve form
Chr17:44073978 A>C (K257T)	Frontotemporal dementia, Pick's disease		Neurons	Tau with this mutation is characterised by less ability to promote microtubule assembly. Diffuse hyperphosphorylated tau in the soma of neurons in the temporal lobes.
Chr17:44073986 A>G (I260V)	Frontotemporal dementia, Pick's disease	Pathologic only in 4R isoforms of tau	Neurons	Selective increase in tau aggregation. Neurodegeneration with gliosis and frontal lobes atrophy
Chr17:44074004 C>G (L266V)	Frontotemporal dementia	4R isoforms of tau	Neurons, glia (mostly astrocytes)	Increase protein level containing 4R tau, lower levels of tubulin polymerization, gliosis after the loss of neurons.
Chr17:44087690 T>G (N279K)	Familial frontotemporal dementia.	Insoluble fraction is mostly in 4R	Neurons, glia	The most frequent mutation in familial frontotemporal dementia with Parkinsonian features. Pathological forms of tau deposition in the medial temporal cortices, upper and lower motor neurons.
Chr17:44087741 T>C (N296N)	Frontotemporal dementia, supranuclear palsy	Increased 4R:3R ratio	Neurons	Loss of neurons with tau inclusions in the globus pallidus, substantia nigra, and locus ceruleus

Chr17:44087754 C>A (P301T)	Globular glial tauopathy, frontotemporal dementia	4R isoforms of tau	Neurons, astrocytes, oligodendrocytes	Loss of neurons in the frontal cortex, substantia nigra, and spinal cord with astrogliosis and spongiosis.
Chr17:44087754 C>T (P301S)	Frontotemporal dementia		Neurons, glia	Frontotemporal and front-orbital neuronal loss with hyperphosphorylated tau forms, impaired ability to stimulate assembly of microtubules.
Chr17:44087755 C>T (P301L)	Frontotemporal dementia	Mostly 4R isoforms of tau	Neurons, astrocytes, oligodendrocytes	Stimulates the formation of β-sheet structures and paired helical filaments. Atrophy of frontal and temporal lobes, basal ganglia and hippocampus.
Chr17:44087761 G>T (G303V)	Supranuclear palsy	Increase of 4R isoforms of tau	Neurons, glia	Atrophy of the subthalamic nuclei, mesencephalon and striatum with neurofibrillary tangles.
Chr17:44087767 G>A (S305N)	Frontotemporal dementia		Neurons, glia	Presence of ring-shaped neurofibrillary tangles in frontal, temporal, insular, and postcentral cortices.
Chr17:44087768 T>C (S305S)	Frontotemporal dementia, supranuclear palsy	Increase of 4R isoforms of tau	Neurons, astrocytes	Degeneration of the frontal and temporal lobes with gliosis.
Chr17:44087771 G>A (IVS10+3 G>A)	Frontotemporal dementia, supranuclear palsy	Increase of 4R isoforms of tau	Neurons, glia (oligodendrocytes mostly)	Neurofibrillary tangles in the hippocampus, basal ganglia, frontal and temporal cortices, and granular and grain-like deposits of insoluble tau forms.
Chr17:44087772 A>C (IVS10+4 A>C)	Frontotemporal dementia	Increase of 3R isoforms of tau	Neurons	Patients had severe atrophy of the frontotemporal lobes with astrogliosis and relative motor and visual cortex preservation.
IVS10+13 A>G and IVS10+14 C>T	Frontotemporal dementia	Increase of 4R isoforms of tau	Neurons, glia (oligodendrocytes mostly)	Severe "knife-edge" atrophy in the frontal and temporal lobes. Neurodegeneration in the substantia nigra and amygdala is compensated by gliosis.
Chr17:44087787 C>G (IVS10+19 C>G)	Frontotemporal dementia	Increase of 3R isoforms of tau	Neurons	The patient has atrophy of the frontotemporal lobes.

Chr17:44091644 G>C (K317N)	Frontotemporal dementia	4R and 3R forms have different consequences	Neurons, astrocytes and oligodendrocytes	Patients had lobar atrophy with gliosis and cognitive impairment, and parkinsonism symptoms. Accelerated tau assembly in 4R tau while decreasing tau aggregation, misfolding, and filament assembly in 3R tau.
Chr17:44091652 C>T (S320F)	Frontotemporal dementia		Neurons, glia (oligodendrocytes mostly)	Neurodegeneration was observed in the temporal lobes (with gliosis), cingulate gyrus, entorhinal cortex and hippocampus. The mutation's consequence is removing a potential phosphorylation site in tau.
Chr17:44091652 C>T (P332S)	Frontotemporal dementia	4R and 3R forms	Neurons	Atrophy of primary motor and premotor cortices with 3R and 4R tau aggregates. Reduced capacity to bind microtubules for tau.
Chr17:44095989 G>A (G335S)	Frontotemporal dementia		Neurons, glia (oligodendrocytes mostly)	Loss of neurons in the frontal and temporal lobes, hippocampus or/and substantia nigra. Reduced capacity to bind microtubules for tau.
Chr17:44095993 A>G (Q336R)	Frontotemporal dementia, pick's disease	4R and 3R forms	Neurons, glia (oligodendrocytes mostly)	An increase in tau fibrillogenesis with gliosis was observed, followed by an increase in tau fibrillogenesis.
Chr17:44095995 G>A (V337M)	Frontotemporal dementia	Typical for 4 R forms	Neurons	In the presence of a mutation, there is an increase in the phosphorylation of sites in the 4P forms of tau. Tangles were found in the neocortex, amygdala, and parahippocampal gyrus.
Chr17:44101439 A>C (N410H)	Frontotemporal dementia	Increase in the 4R:3R ratio	Neurons, glia astrocytes, mostly	The increase of tau filament formation but the reduction in microtubule polymerization. Mild forms of neuronal loss in the frontal cortex.

Tau isoforms display differences in aggregation properties. Rates of assembly between 4R and 3R tau isoforms are distinct, with 4R tau isoforms assembling 2.5–3.0 times more rapidly compared to 3R tau isoforms, with no contributions by differences in amino-terminal insertions (Goedert and Jakes, 1990). These differences in the assembly of 4R compared to 3R tau isoforms indicate variations in the kinetics of aggregation of 4R compared to 3R tau isoforms. Differences in aggregation properties of tau isoforms implicate heterogeneity in the compositions of tau aggregates among tauopathies expressing altered ratios of 4R and 3R tau isoforms. The shortest tau isoform 0N3R is present in the human fetal brain and has the highest number of phosphorylated sites relative to the full protein length. It cannot polymerize into NFTs and form aggregates under natural conditions (Yu et al., 2009).

The samples from patients and experiments with seeding in HEK biosensor cells showed the presence of different modifications, but most were related to phosphorylation on T231 and S235 or S262. The role of phosphorylation in tau uptake is also not completely understood. Hyperphosphorylation of tau is considered an early sign of pathology, as it can reduce the affinity of tau for microtubules, becoming one of the factors leading to aggregation. Experiments demonstrated that extracellular tau can be hypo-phosphorylated. Other studies showed the opposite results, such as adding phosphoryl group to S199 or S404 amino acid residues. In parallel, dephosphorylation of the same regions can decrease tau uptake (Takeda et al., 2015). Searching for seed-containing exosomes showed forms of tau that were posttranslational modified at S396 and T181 (Dujardin et al., 2021; Han et al., 2017; Wang et al., 2017).

There are 85 phosphorylation sites (44 for S, 35 for T and 5 for T), so phosphoryl molecules can be added to almost 20 % of amino acid residues during hyperphosphorylation. Forty-four phosphorylation sites were found to be phosphorylated in tauopathies at a higher frequency than normal. Most of the phosphorylation sites are located in the microtubule-binding domain. Hyperphosphorylation in other parts of the protein sequence does not impair the ability to bind with tubulin but can change the efficiency of the aggregation process. Some of these residues undergo phosphorylation in the normal healthy brain with age and do not lead to noticeable damage. Many amino acid residues are part of signal sequences leading to protein degradation or are located in close proximity to ubiquitination sites (Alquezar et al., 2021). Based on the above, it can be assumed that different levels of phosphorylation in the selected regions of the tau protein may play a key role in the pathological transformation of tau from a biologically active molecule to a molecule that inhibits microtubule assembly.

Recombinant wild tau can be uptaken by closely spaced neurons, supporting the hypothesis that tau can move from neuron to neuron under healthy conditions. Whether this is a signaling pathway or just a product of catabolism and a damaged protein clearance mechanism remains unclear. It can be assumed that physiological tau will be distributed as a monomer since the formation of tau aggregates is considered a pathological event. However, it has recently been shown that some form of tau-tau self-interaction exists during microtubule binding and stabilization under physiological conditions (De La-Rocque et al., 2021).

Studies demonstrated that 2 hexapeptides, VQIINK (located in R2) and VQIVYK (located in R3), are capable of self-assembly, leading to the formation of physiologically insoluble β-sheet-rich fibrils. However, they cannot form fibrils competent for seeds (Annadurai et al., 2022a, 2022b). However, the R3 region is capable of self-aggregation and forming competent fibrils. Even after the breakdown of protein regions into smaller parts, R2 and R3, they can form seed-competent fibrils when an inducer is added. R3 is capable of fibrillation even without adding inducers, such as heparin. At the same time, replacing one amino acid in R3 eliminates its ability to self-aggregate and form seeds. Tau RD P301S biosensor cells and Tau P301L expressing HEK293 cells seeded with R2 and R3 fibrils showed induction of abnormal tau phosphorylation at positions Ser262/Ser396/Ser404. Moreover, protein fractions isolated from biosensors seeded with R2 and R3 fibrils can transfer endogenous tau to their neighbors when naive HEK293 is added to the culture.

3.1.2 Tau Interactions in Healthy and Pathological Conditions

Tubulin-Associated Unit (tau) is a microtubule-associated protein highly expressed in neurons and is usually redistributed with preference from the soma towards the axons. Tau plays a key role in the functioning of neurons: from the differentiation of neuroblasts to the formation of long-term memory. The coordinated work of protein systems is necessary to perform complex functions, including microtubule plus-end tracking proteins and other microtubule-associated proteins (Biundo et al., 2018; Sayas and Ávila, 2014).

There are two opinions in the literature on the role of tau in microtubule stabilization. In the first case, authors write that tau stabilizes microtubules in the axon (Caceres and Kosik, 1990; Kadavath et al., 2015; Qiang et al., 2018). There is evidence that the destabilization of microtubules can be caused by a lack of tau (Brunden et al., 2014). According to another theory, because tau is found in a more significant amount in the labile domain, it does not meet the criteria of a stabilizer. When the tau level is artificially decreased in animal models, the mass of labile microtubules in axons decreases in parallel, but the mass of stable microtubules increases. It is an agent that allows the microtubules to have long labile domains for longer. The role of a true stabilizer for microtubules is played by MAP6 (Liu et al., 2019).

Together with a decrease in tau, the level of mitochondrial lability decreases with a parallel increase in the number of their abnormal forms. The mechanism of this relationship is not known (Sapir et al., 2012). Models show a positive correlation between tau knockout and neuronal outgrowth (Liu et al., 2019), tau knockout and density of microtubules in axons of small diameter (Harada et al., 1994), increasing velocity of mitochondrial axonal transport as a result of the exclusion of 4R tau forms by genetic methods (Beevers et al., 2017). Knockout models also show a decrease in labile microtubule mass, with an increase in the stable domain, an increase in neuronal branching(Yu et al., 2008), long-term depression and long-term potentiation deficit(Ahmed et al., 2014; Kimura et al., 2014), decrease in apical and basal dendrite density, even during short-term knockouts (Velazquez et al., 2018), the impaired repulsive response of the growth cone (Biswas and Kalil, 2018), disruption to axonal extension, and delayed neuronal maturation (Dawson et al., 2001; Kent et al., 2020).

3.1.3 Mechanisms of TAU Spreading

Tau can be spread through microvesicles or exosomes (Saman et al., 2012) following cell death by autophagosomes (Mohamed et al., 2014). Seeds can get inside a healthy cell without the preliminary formation of lipid vesicles (Merezhko et al., 2018). Hyperphosphorylated forms of tau were found in the cerebrospinal fluid of patients with AD, even in the early stages of the disease and are considered biomarkers(Pernègre et al., 2019). Because tau lacks the N-terminal conventional signal peptide sequence, pathological tau forms can use only Type I and III of unconventional protein secretory systems. The first one allows the transport of seeds across the plasmalemma and functions as a vesicular body-assisted secretion system (Cruz-Garcia et al., 2020). Extracellular tau can be uptaken by neurons with the help of micropinocytosis. This process depends on interactions with heparan sulfate proteoglycans (Holmes et al., 2013).

The propagation of protein aggregates along anatomically related pathways does not need external inducers. A functioning model was created (Demaegd et al., 2018) that is analogous to the mechanisms of prion propagation due to the similar characteristics of the induction of abnormal protein conformation. Microglia is another possible tau spreader, as depletion of microglial cells can suppress tau propagation and reduce excitability in the dentate gyrus in a mouse model.

3.2 Cell Cultures in Modeling

3.2.1 Neuronal Component

The use of primary neurons derived from embryos of mammals is limited by the absence of division possibility of mature neuronal cells, which is further complicated by economic factors and ethical issues. Neurons obtained from iPSCs are time-consuming and demanding for the exact selection of the components of the cultivation and differentiation medium, but also require subsequent more detailed selection of cells according to differentiation markers due to frequent mixing of the final culture. Induced pluripotent stem cells can be used as an appropriate replacement. Transformed neuron-like cell lines are much cheaper and theoretically require less time to reproduce the conditions of normal or pathological parts of the brain tissue. Additional advances are relatively easy genetic modifications and human origin, which means expressing proteins and their isoforms not inherently present in rodent primary neurons or cell lines.

SH-SY5Y cells were chosen for mimicking adult neurons because N-types of these cells express some neuronal markers and show higher levels of mature neuronal biomarkers after induction. Its direct precursor comes from neuroblastoma cell lines, subcloned 3 times. As a result, an epithelial-like line S and a neuron-like line N appeared. After differentiation into neuron-like cells, SH-SY5Y exhibit a polarity, an important characteristic of neuronal lineage. We can also observe neurites outgrowths, the expression of the neuronal maturation markers such as βIII-tubulin, mature isoforms of TAU, synaptophysin (Sph), Choline Acetyltransferase

(ChAT) and Microtubule-Associated Protein 2 (MAP2), and induce TAU aggregation (Bell and Zempel, 2022; de Medeiros et al., 2019; Martin et al., 2022). There is also information in the literature about basal noradrenaline release and tyrosine hydroxylase (TH) activity (Khwanraj et al., 2015; Xicoy et al., 2017). It is also known that the N-terminal half of the TAU is insufficient for axonal targeting because the N-term-TAU is not axonally enriched. Differentiated cells of this cell line do not form classical axon initial segment formation due to the absence of ankyrin G and TRIM46 in the proximal axon. That suggests that successful TAU sorting in axons does not depend on the axonal initial segment formation (Bell et al., 2021).

The disadvantages of undifferentiated cells for creating models are as follows:

(1) The doubling time of neuroblastoma cells is close to 27 hours. Cell cycles are not synchronized, which can cause problems in assessing neurotoxicity due to the impossibility of differentiating and defining the cause of changes in the cell number during treatment with neuroprotective or neurotoxic compounds for testing their abilities under different conditions (Kovalevich and Langford, 2013).

2) Cells in culture do not always have the same phenotype (especially in mediums with a different serum which cannot be precisely standardized), and the expression of neuronal biomarkers can be on different levels and change during the experiment, which may lead to inaccurate results.

3) Differentiated and non-differentiated cells can show different sensitivity to the treatment, and that can affect the results. A population of undifferentiated cells can have a set of cells with neuronal phenotypes due to spontaneous regression, which is prominent in neuroblastoma (Brodeur, 2018).

4) Even when cells express some biomarkers typical for mature neurons, such as TH, cells could be incapable of synthesizing other essential components of the biochemical pathway (dihydroxyphenylalanine decarboxylase or other enzymes) (Xie et al., 2010).

During the search for a protocol for cell cultivating and differentiation, several inconsistencies were found:

1. Differences in types of cultivation and differentiation medium
2. Variations in types and percentages of serum
3. Differences in cell source
4. Disagreement in final cell differentiation results or levels of expression of biomarkers

Another issue is associated with dopamine production by the SH-SY5Y line under differentiated and undifferentiated conditions. Recent studies show the same level of TH expression in RA-treated and undifferentiated cells (Alrashidi et al., 2021). Others have shown the necessity of adding an L-DOPA supplement for dopamine synthesis (de la Fuente et al., 2017). Further sources demonstrate basal dopamine production in undifferentiated SH-SY5Y line with a significant level of TH expression (Khwanraj et al., 2015). At the same time, differentiation with trans-retinoic acid can cause an increase in the expression of TH and

dopamine transporters but, at the same time, leads to lower levels of vesicular monoamine transporter (Presgraves et al., 2003).

The most important step could be the choice of a medium. For example, using Dulbecco's Modified Eagle Medium (DMEM) or Roswell Park Memorial Institute medium can change the metabolome of a cell line through nutrient availability or the oxygenation level. The intracellular concentration of pyruvate, glutamate, α-ketoglutarate or proportion of NAD/NADH can affect epigenetic mechanisms of gene expression and differentiation process through histone-lysine demethylases (Xicoy et al., 2017).

Considering the presence of potential growth factors, hormones, and small bioactive molecules that can influence the differentiation of neuroblastoma, serum from different species or variations in Fetal Calf Serum (FCS) batches from different companies or even batches received from the same company may influence the result. NBM was used to prevent those effects of unknown factors from serum. Evidence shows the possibility of replacing FCS with a B-27 supplement and L-glutamate. However, information regarding the B-27 supplement was found contradictory due to the consistency of the ratio of components and the purity of the product offered by the manufacturer (Chen et al., 2008). Medium supplements such as B-27 also can be used for neuroblastoma differentiation by themselves (Martin et al., 2022). Cells older than 30 passages were not used for experiments to eliminate the effect of senescence. In the case of the neuroblastoma cell line, senescence causes the accumulation of ROS oxidation byproducts (Strother et al., 2021).

There is also contradictory information showing that the SH-SY5Y line can respond inconsistently to the same differentiation initiation, depending on the source, passage number and stress (Wang et al., 2007; Xicoy et al., 2017). Neuroblastoma can also behave like the neuronal-like culture on different surfaces without adding any differentiation agents (Dwane et al., 2013). The most popular differentiation agent, retinoic acid (RA), can affect the cell line through retinoic acid receptors in the nuclear compartment that can dimerize with the retinoic X variant of receptors after activation. Through retinoic acid response, element activation of transcription is started. An important role is played by most of the pathways related to the second type II of protein kinase A. Brain-Derived Neurotrophic Factor (BDNF) can bind to the neurotrophin receptor p75 or the tyrosine kinase receptors leading to activation of the TrkB pathway (Joshi et al., 2006; Kumawat and Gosens, 2016; Nagpal and Wei, 2019; Qiao et al., 2012; Xie et al., 2010).

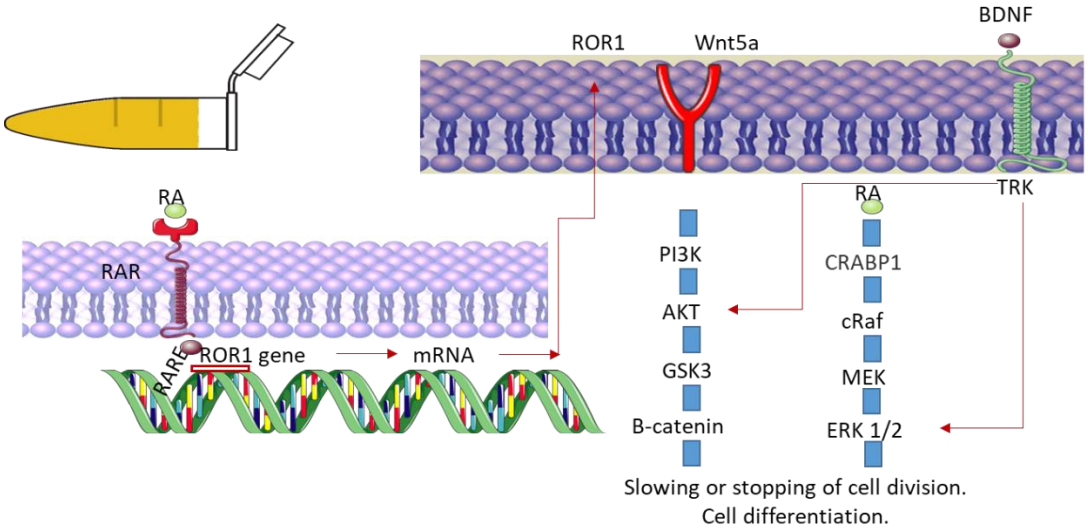

Figure 3.2. SH-SY5Y differentiation model with RA and BDNF treatment. RA binds to RAR and migrates into the nucleus, binding on Retinoic Acid Response Element (RARE) sequence. It increases ROR1 and Wnt5a synthesis, and the ROR1 signaling pathway cascades. RA also can influence through cellular retinoic acid binding protein 1 (CRABP1), leading to incomplete activation of ERK 1/2.

Neurite elongation in the SH-SY5Y line is regulated by at least 14 genes influenced by trans-RA activity. Wnt signaling pathway is important for preventing cell division and changes in response to insulin and neurotrophin factors (Merrill et al., 2004). In this regard, the highest priority is optimising the cell density in the flask, which can affect the pathways leading to differentiation according to one scenario or another.

SH-SY5Y is popular for modeling the conditions for the formation of amyloid plaques, tau hyperphosphorylation and the spread of pathological forms of tau in the extracellular environment in 2D culture. This is important due to the necessity to find ways of crossing both pathological mechanisms in neurons (Roda et al., 2022). Also, there is a lack of signficicant studies on using SH-SY5Y in spheroids models. Evidence from the literature shows the following trend of expression of Sph biomarker: non-treated cells in 2D culture < non-treated spheroids < cells in 2D culture after differentiation or changing the state to quiescent < differentiated spheroids 3D culture (Jung et al., 2013).

Critical information for the study was also the difference between the expression of tau-isoforms under untreated and differentiated conditions. Untreated neuroblastoma can express mRNA of tau exons 2 and 10. The minimum required condition to detect products from exon 3 is RA treatment. Different mature neuron markers and enforcement of pathological tau formation by treatment with okadaic acid in 3D, which can be achieved relatively easily after genetic modification of normal SH-SY5Y cell line, are known for neurodegenerative disease modeling (Seidel et al., 2012).

Growing cells in a 3D culture are important not only for the apparent reasons of eliminating the influence of the polymer basis to which adherent 2D cultures are attached, simplifying access to nutrients and lower cell density. 3D co-culture conditions reflect normal intercellular

interactions with the complex mutual influence of neurotrophic factors. Studies comparing 2D and 3D cultures of SH-SY5Y found that β III-tubulin expression was significantly higher under three-dimensional conditions. Treatment with BDNF in 3D changed the localization of tau and created prerequisites for interaction with other cytoskeleton elements. SH-SY5Y cell line expressed tau isoforms with neuronal localization typical for mature neurons. All these points favour the advantage of choosing a three-dimensional cell culture for modeling AD and tau seeding in particular (Agholme et al., 2010).

3.2.2 Glial Component

As the glial component, astrocytes are the most common cell type in the CNS. They play a significant role in neurovascular coupling and protect the surrounding cells from stressful conditions and enwrapping synapses. There is evidence that astrocytes respond to NFTs and plaques in AD, but it is still unclear under which conditions their effect is neuroprotective or harmful. Astrocytes also have a waste clearance role known as glymphatic, in which perivascular channels facilitate the efficient removal of soluble proteins and metabolites, including β-amyloid, from the CNS. Astrocytes directly contact the CNS vasculature through their terminal processes and dilate or constrict blood vessels to accommodate nutrient and waste exchange, depending on total activity. But there is not enough information if they can transport potentially harmful compounds in AD. Type 4 aquaporin also plays a vital role in the clearance and exchange of solutes in a water-dependent manner between the cerebrospinal fluid compartment and extracellular fluid (Monterey et al., 2021).

Astrocytes respond to most of the known pathological environment of the central nervous system, including AD. It is accompanied by forming a heterogeneous population at different stages of the disease with changes at a molecular level. This condition is known as "reactive astrocytes". Astrocytes were previously thought to contribute to neuronal degeneration by releasing pro-inflammatory mediators. Astrocytes with hypertrophied phenotype were found in the neurofibrillary tangle stage of AD with a higher level of Glial Fibrillary Acidic Protein (GFAP) expression. Spiky tau+ astrocytes are a feature of brain aging. The inclusions can be fibrillary tau and immunohistochemical, and tests showed the 4-repeat tau nature of them. Of particular note is the relationship between the accumulation of pathological forms of tau in the brain of AD patients and the detection of GFAP in the cerebrospinal fluid (Ferrari-Souza et al., 2022). GFAP is involved in cytoskeleton assembly and maintaining cytoskeleton integrity. It is expressed in mature astrocytes and is known to be neuroprotective, as GFAP knockout mice are susceptible to brain injury caused by trauma and inflammation. GFAP hyperphosphorylation and other post-translational modifications play an important role in protein aggregation. For example, hippocampus GFAP is detected without phosphorylation and/or oxidation in age-matched control in AD. Experiments also showed that AD-specific phosphorylations by RNAi knockdowns of GFAP could reduce amyloid deposition in glioma and neuroblastoma lines, increasing interest in creating cellular models which will include an astrocytic and neuronal component (Ganne et al., 2022).

There is a lack of well-described protocols for differentiating gliomas and astrocytomas to mature astrocyte phenotype in the literature, but authors suggest using agglutinins and synthetic substances associated with the metabolism as cAMP. The appearance of CD44, Aquaporin-4 and GFAP are the most popular markers for determining proximity to mature astrocytes. Astrocytic differentiation in normal tissue goes through phosphorylation of JAKsin that causes activation of STAT3 followed by redistribution of dimers to the nucleus and regulation of genes responsible for stem-cells renewal (Sasaki et al., 2002; Welch et al., 1995).

The released Notch intracellular domain binds to the hairless (RBP-J) suppressor, which initiates Notch target gene transcription (Pavlou et al., 2019). Signaling through the Notch pathway promotes the transition of undifferentiated cells towards glial cells, while neurogenesis and the differentiation pathway into oligodendrocytes are, on the contrary, suppressed. In glioma cell lines, lectins can inhibit proliferation. After binding to glycans with N-acetyllactosamine repeat units, Datura stramonium agglutinin causes the proliferation of SNB-75 cells to stop (Sasaki et al., 2002).

3-isobutyl-1-methylxanthine (IBMX) functions as a non-specific inhibitor of adenosine 3',5'-cyclic monophosphate phosphodiesterase, which leads to the increase of cAMP following activation of Protein kinase A (PKA). PKA can affect the proliferation and differentiation of cancerous cells and induce apoptosis. Dibutyryl cAMP increases tyrosinase activity and, in combination with the effect of IBMX and RA through the cAMP response element in the PGC-1α proximal promoter, leads to the differentiation of a malignant cell line (Chen et al., 1998; Elks and Manganiello, 1985; Tio et al., 2010).

4 MATERIALS AND METHODS

4.1 Cell Lines

SH-SY5Y cell line (ATCC)

SNB-75 cell line (ATCC)

SH-SY5Y cell line modified with Tau.K18 (P301L/V337M), pMK1253 (Plasmid #133058, Addgene)

SNB-75 cells modified with DsRed, Plenti-CMV-MCS-RFP-SV-puro (Plasmid #109377, Addgene)

Tau RD P301S FRET Biosensor cells (ATCC)

4.2 Instruments and Software

Biological safety cabinets Class II (Hera safe, Thermo Fisher Scientific)

Bio TDB-100 Dry Block Thermostat (Biosan, Latvia)

BRANSON sonicator

Cell Voyager CV7000S (Yokogawa, Japan)

CellCarrier and PhenoPlate 96 well microplates (PerkinElmer, USA)

CellCarrier Spheroid ULA 96-well microplate (PerkinElmer)

CellCarrier 384-well plates (PerkinElmer, 6057308)

CellVoyager High-Content Imaging System (CV7000, Yokogawa Electric Corporation)

Centrifuge 5810R (Eppendorf, Germany)

Centrifuge Rotina 420 R (Hettich Zentrifugen, Germany)

ChemiDoc MP analyser (BioRad, USA)

Confocal microscope Carl Zeiss LSM 780 with UV laser and ELYRA.PS1 module (Zeiss, Germany)

Electrophoresis and Blotting Vertical Apparatus (BioRad, USA)

Eppendorf® ep Dualfilter T.I.P.S.® (Sigma-Aldrich)

Fluorescence microscope Axio Observer D1 (Zeiss, Germany)

Light microscope CK2 (Olympus, Japan)

Multidrop™ Combi Reagent Dispenser (Thermo Fisher Scientific)

Microplate Washer Dispenser (EL406, BioTek)

PerkinElmer Enspire ™ Microwell plate reader

Rotator SB3 (Stuart, UK)

Single channel microliter pipettes Eppendorf Research® plus (Eppendorf, Germany)

Small Tube Dispensing cassette with metal tips (24073295, Thermo Fisher Scientific)

Standard Tube Dispensing Cassette with plastic tips (24072670, Thermo Fisher Scientific)

Sterile Conical Tubes (SPL LIFE SCIENCES, the Republic of Korea)

Thermo-Shaker PST-60HL (Biosan, Latvia)

ViCell XR Cell Viability Analyzer (Beckman Coulter Inc., USA)

Vortex - Lab Dancer (IKA, Germany)

Water bath (Memmert, Germany)

4.3 Chemicals and Solutions

10x Tris/Glycine/SDS (Bio-Rad, #1610772)

30 % Acrylamide/Bis-acrylamide 29:1 (Bio-Rad, #1610156)

3-ISOBUTYL-1-METHYLXANTHINE (Merck Life Science spol. s r.o., #I5879-100MG)

CTS™ Neurobasal™ A Medium 1X (Thermo Fisher Scientific)

Dimethyl Sulfoxide (DMSO) (Sigma, #D4540)

DMEM (Lonza, #12-604F)

FCS (Capricorn Scientific)

Gibco™ B-27™ Supplement (50X), serum-free: (ThermoFisher Scientific, #17504044)

Hoechst-33342 (Invitrogen, #H21492)

Lipofectamine™ 3000 Transfection Reagent (Thermo Fisher Scientific, #L3000015)

Low melting agarose (#A9414, Sigma-Aldrich)

L-glutamine (Thermo Fisher Scientific, #16600082)

N6,2′-O-Dibutyryladenosine 3′,5′-cyclic monophosphate sodium salt, (Merck Life Science spol. s r.o., #D0627-100MG)

Opti-MEM™ I Reduced Serum Medium 1X No Phenol Red (Thermo Fisher Scientific, #11058021)

Penicillin-Streptomycin (Thermo Fisher Scientific, #15140163)

PhosSTOP™ (Roche, #04906845001)

Pierce™ BCA Protein Assay Reagent A (Thermo Scientific, #23223)

Pierce™ BCA Protein Assay Reagent B (Thermo Scientific, #23224)

Polybrene (TR-1003-G, Merck)

Protease Inhibitor Cocktail Tablets (Roche, #04693116001)

Recombinant Human BDNF Protein, (R&D Systems, Inc. a Bio-Techne Brand, #248-BDB-250)

Resolving gel buffer 1.5 M Tris-HCl pH 8.8 (Bio-Rad, #161-0798)

Spectra™ Multicolor Broad Range Protein Ladder (Thermo Fisher Scientific, #26634)

Stacking gel buffer 0.5 M Tris-HCl pH 6.8 (Bio-Rad, #161-0799)

TEMED (Bio-Rad, #1610801)

TrypLE™ Express recombinant cell dissociation reagent (Thermo Fisher Scientific, #12604021)

Ethanol (Merck, #100983).

Media:

Differentiation Medium #1 (DMEM with 1 % FCS, 1 % antibiotics and 10 μM RA)

Differentiation Medium #2 (NBM with 10 μM RA)

Differentiation Medium #3 (DMEM with 1 % FCS, 1 % antibiotics,10 µM RA and 50 ng/ml BDNF)

Differentiation Medium #4 (NBM with 10 µM RA and 50 ng/ml BDNF)

Differentiation Medium #5 (NBM with 10 µM RA, 0.25 mM IBMX and 0.5 mM dibutyryl cAMP)

Differentiation Medium #6 (NBM with 10 µM RA, 50 ng/ml BDNF, 0.25 mM IBMX and 0.5 mM dibutyryl cAMP)

Differentiation Medium for SNB-75 cells (NBM with 0.25 mM IBMX and 0.5 mM dibutyryl cAMP)

Western Blot Chemicals:

10x PBS: 80 g NaCl, 2.0 g KCl, 14.4 g Na_2HPO_4, 2.4 g KH_2PO_4 dissolved in 800 ml dd H2O, pH adjusted to 7.4 with HCl and added ddH_2O to 1 l, sterilized by autoclaving.

10x TBS buffer: 24 g Tris base added with 88 g NaCl to 900 ml dd H_2O. pH should be adjusted to 7.6 with HCl and added dd H_2O to 1 l.

TBST: mixed TBS with dd H_2O (1: 9) and 0.1 % Tween20. Because of the high density, it is necessary to cut off 0.5 cm of the tip and aspirate Tween20 slowly.

RIPA buffer: 150 mM sodium chloride, 1.0 % NP-40, 0.5 % sodium deoxycholate, 0.1 % SDS, 50 mM Tris, pH 8.0.

5× SDS loading buffer: 250 mM Tris-HCl (pH=6.8), 10 % SDS, 30 % glycerol, 0.5 M DTT, 0.02 % bromophenol blue, 10 % mercaptoethanol.

0.05 % Triton X-100 solution (10 mL): 1X TBS with 5 µL Triton X-100.

10 % SDS: 100 g of SDS dissolved in 800 mL of dd H_2O, then dd H_2O added to 1 L.

5 % Bovine Serum Albumin (BSA) blocking solution: 5 g BSA dissolved in 100 ml TBST buffer.

8 % resolving polyacrylamide gel (20 mL for 2 1.5 mm thick gels): 9.2 ml dd H_2O, 5.2 ml 30 % acrylamide/bis-acrylamide, 5.2 ml resolving gel buffer, 200 µl 10 % (w/v) SDS, 200 µl 10 % (w/v) Ammonium Persulphate (APS), 20 µl TEMED.

10 % resolving polyacrylamide gel (20 mL for 2 1.5 mm thick gels): 7.6 ml dd H_2O, 6.8 ml 30 % acrylamide/bis-acrylamide, 5.2 ml resolving gel buffer, 200 µl 10 % (w/v) SDS, 200 µl 10 % APS, 20 µl TEMED.

Stacking polyacrylamide gel (5 mL for 2 1.5 mm thick gels): 2.975 ml dd H_2O, 670 µl 30 % acrylamide/bis-acrylamide, 1.25 ml stacking gel buffer, 50 µl 10 % (w/v) SDS, 50 µl 10 % APS, 5 µl TEMED.

Transfer buffer **(**1 l): 200 ml of 5x Transfer buffer, 200 ml 96 % ethanol, 600 ml ddH2O.

Spheroids Fixation and Immunostaining Reagents:

Blocking mixture: 5 % BSA, 1 % Goat Serum Albumin (GSA) and 1 % Donkey Serum Albumin (DSA) (to the final volume of the solution) should be added to the mixture of Buffer #1 and 10 % DMSO and vortexed.

Buffer #1 (500 ml): 50 ml of 10x PBS and 1 ml of Triton X-100 should be solved in 449 ml of dd H_2O.

Buffer #2 (500 ml): 50 ml of 10x PBS. 1 ml of Tween20 and 0.5 ml of heparin should be solved in 448,5 ml of dd H_2O.

Fixation buffer (250 ml): 220 ml of dd H_2O, 5 ml of DMSO and 25 ml of 37 % formaldehyde should be mixed. 1.5 g Na_2HPO_4 and 1.13 g NaH_2PO_4 should be added and dissolved in the mixture. The fixation buffer should be kept protected from direct light. All the manipulations should be done with nitrile gloves.

Permeabilization buffer (50 ml): 40 ml of Buffer #1, 1.65 g of glycine and 10 ml of DMSO should be mixed and vortexed.

Antibodies:

Anti-GAPDH Mouse Monoclonal Antibody (Santa Cruz Biotechnology, #sc-32233), 1:4000

Anti-Tau5 Mouse Monoclonal Antibody (Thermo Fisher Scientific, #AHB0042), 1:1000

Anti-Phospho-Tau (Ser262) Rabbit Polyclonal Antibody (Thermo Fisher Scientific, #OPA1-03142), 1:1000

Anti-β3-Tubulin (D71G9) XP® Rabbit Monoclonal Antibody (Cell Signaling Technology, #5568)

Anti-GFAP (Glial fibrillary acidic protein Antibody) (D1F4Q) XP® Rabbit Monoclonal Antibody (Cell Signaling Technology, #12389)

Anti-Synaptophysin (D8F6H) XP® Rabbit Monoclonal Antibody (Cell Signaling Technology, #36406)

Anti-MAP2 Polyclonal Rabbit Antibody (Cell Signaling Technology, #4542)

Anti-hChAT (Human Choline Acetyltransferase) Goat Polyclonal Antibody (Novus Biologicals, LLC #AF3447)

Anti-TH (Tyrosine Hydroxylase) Polyclonal Sheep Antibody, (Novus Biologicals, LLC, #AF7566)

Rabbit Anti-Sheep IgG Antibody, HRP conjugate (Sigma-Aldrich, #AP147P), 1:2000

Donkey anti-Mouse IgG (H+L) Highly Cross-Adsorbed Secondary Antibody, Alexa Fluor™ 488 (Thermo Fisher Scientific, #A21202), 1:2000

Donkey anti-Goat IgG (H+L) Cross-Adsorbed Secondary Antibody, Alexa Fluor™ 488 (Thermo Fisher Scientific, #A11055), 1:2000

Goat anti-Rabbit IgG (H+L) Highly Cross-Adsorbed Secondary Antibody, Alexa Fluor™ 488 (Thermo Fisher Scientific, #A11034), 1:2000

Goat anti-Rabbit IgG (H+L) Cross-Adsorbed Secondary Antibody, Alexa Fluor™ 647 (Thermo Fisher Scientific, #A21244), 1:500

Goat anti-Mouse IgG (H+L) Cross-Adsorbed Secondary Antibody, Alexa Fluor™ 594 (Thermo Fisher Scientific, #A21244), 1:500

VGLUT1 Antibody (S28-9) Mouse Monoclonal Antibody (Novus Biologicals, LLC #NBP2-59329)

4.4. Software:

Columbus Image Data Storage and Analysis System, ver. 2.7

ImageJ, ver. 1.4.3.67

GraphPad Prism (GraphPad, USA)

ZEN 2012 (blue edition)

4.5 Methods

4.5.1 Cell Culturing

SH-SY5Y, SNB-75 and Tau P301S biosensor cells were kept in filtered complete DMEM with 10 % FCS and 1 % streptomycin and penicillin in a humidified incubator with 5 % CO_2 at 37°C. Cells were passaged every 2-3 days after confluence was reached. For passaging, cell lines were washed with PBS and detached with TrypLE (2 ml for T-75 or 1 ml for T-25 flask, then 4-5 min of incubation in an incubator). For TrypLE inactivation DMEM with 10 % of serum in 2.5:1 proportion to TrypLE was added. The cells were centrifuged at 1500 RPM for 5 min. The old medium was discarded, a new complete DMEM was added, and cells were resuspended, avoiding getting air inside the tip. Cell number and viability were checked with ViCell XR Cell Viability Analyzer. Only the attached type of cells was used for further cultivation because floating cells were eliminated.

4.5.2 Lentiviral Transduction

Fifteen million HEK 293T/17 cells were plated in a T-75 flask in DMEM with 10 % FCS. The cells were incubated at 37°C, 5 % CO_2 for 24 h. Vectors were added to 1.5 ml of jetPRIME buffer and vortexed with low speed. 90 µl jetPRIME reagent was added to the mix and vortexed at low speed for 10 s. Then the mixture was centrifuged at 300x g for 2 min and incubated for 30 min at RT. The old culture medium was replaced with 10 ml fresh growth media containing the transduction mixture. After 16 h of culture, the old media containing the transduction mixture was replaced with 20 ml of fresh growth media. The cells were then allowed to grow for 72 h to allow viral production before harvesting the virus-containing media.

Intended for modification cell line was plated 2 d after the transfection of 293T/17 cells. The 293T/17 cells medium was collected and centrifuged for 5 min at 300g. Then supernatant was filtered through a 0.45 µm filter. The medium was removed and changed to the lentiviral mixture with 8 µg/ml polybrene added, and the cell line was left for incubation overnight. The complete medium was changed the next day. The selection of the cells with higher expression of protein with fluorescent modifications is recommended in the next 3 days.

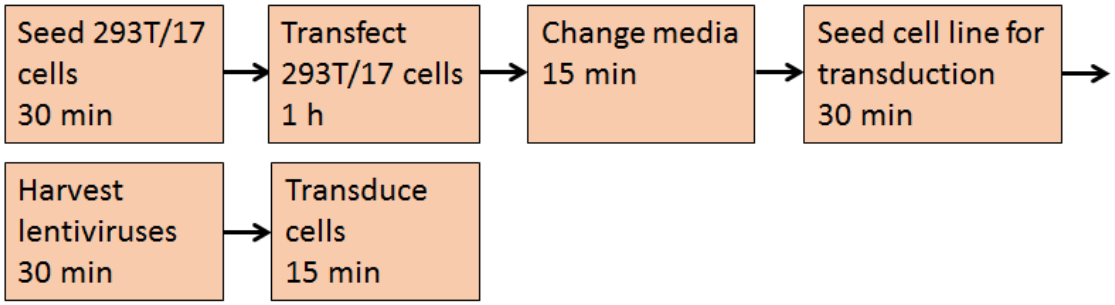

Figure 4.1: Scheme of lentiviral transduction.

4.5.3 SH-SY5Y Differentiation Protocol

Neurobasal medium (NBM): For 100 ml complete medium preparation, 2 ml 0.5 mM L-glutamine and 2 ml B-27 Supplement were added to a filtered Neurobasal™ A in a sterile flow box.

Cells for differentiation were collected in the 15 ml cone tube the same way as during normal passaging, and their number calculated with ViCell XR Cell Viability Analyzer. 0.5 million cells per well were plated in the 6-well plate in a complete DMEM for differentiation in the reduced serum DMEM condition or complete NBM for the differentiation in NBM. Cells were left for attachment and metabolism normalization in the incubator (5 % CO_2 at 37°C) overnight.

24 h after plating, the medium was aspirated, and cells were washed with 1X PBS. The complete medium was changed to the Differentiation Medium #1 (DMEM with 1 % FCS, 1 % antibiotics and 10 µM RA) or the Differentiation Medium #2 (NBM with 10 µM RA). After 72 h, the medium was aspirated, and cells were washed with 1X PBS and changed to the Differentiation Medium #3 (DMEM with 1 % FCS, 1 % antibiotics, 10 µM RA and 50 ng/ml BDNF) or the Differentiation Medium #4 (NBM with 10 µM RA and 50 ng/ml BDNF). Cells can be used for imaging or/and for Western Blot analysis.

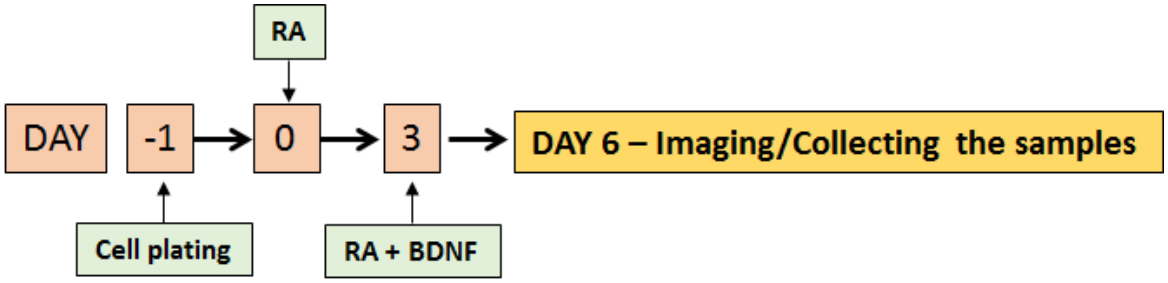

Figure 4.2: SH-SY5Y differentiation protocol.

4.5.3 SNB-75 Differentiation Protocol

Cells for differentiation were collected in the 15 ml cone tube the same way as during normal passaging, and their number was calculated with ViCell XR Cell Viability Analyzer. 0.5 million cells per well were plated in the 6-well plate in complete NBM. The plate was left overnight in the incubator (5 % CO2 at 37°C). 24 h after plating, the medium was aspirated, and cells were washed with 1X PBS. The medium was changed to the Differentiation Medium for SNB-75 cells (NBM with 0.25 mM IBMX and 0.5 mM dibutyryl cAMP).

After 72 h, the medium was aspirated, and cells were washed with 1X PBS. The old medium was changed to the Differentiation Medium for SNB-75 cells (NBM with 0.25 mM IBMX and 0.5 mM dibutyryl cAMP). Cells can be used for imaging or/and for Western Blot analysis.

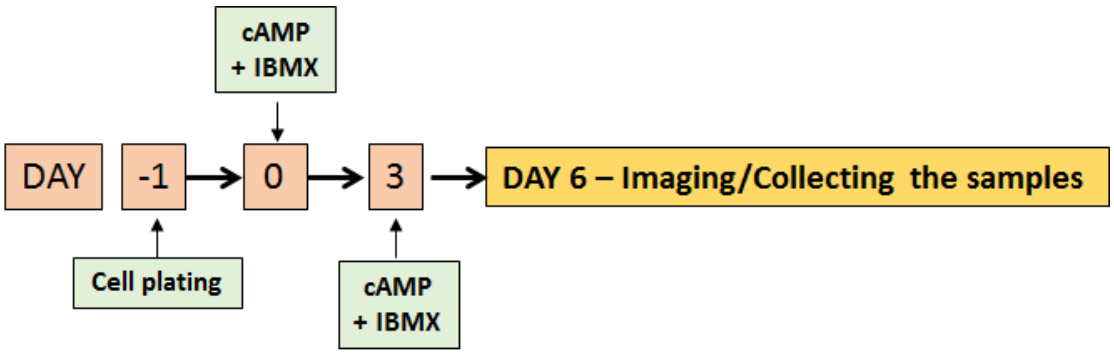

Figure 4.3: SNB-75 differentiation protocol.

4.5.4 Co-culture Differentiation Protocol

To differentiate cell lines in co-culture experiments, 0,5 mln cells were plated in complete DMEM in a ratio of 3 SH-SY5Y (150 000 cells) to 7 SNB-75 (350 000 cells) in the 6-well. The plate was left overnight in the incubator (5 % CO2 at 37°C). 24 h after plating, the medium was aspirated, and cells were washed with 1X PBS. The medium was changed to the Differentiation Medium #5 (NBM with 10 µM RA, 0.25 mM IBMX and 0.5 mM dibutyryl cAMP).

After 72 h, the medium was aspirated, and cells were washed with 1X PBS. The old medium was changed to the Differentiation Medium #6 (NBM with 10 µM RA, 50 ng/ml BDNF, 0.25 mM IBMX and 0.5 mM dibutyryl cAMP). After 6 days of differentiation, cells can be used for imaging or/and for Western Blot analysis.

4.5.5 Spheroids Formation

Before agarose plate coating, 1.5 g of low-melting-point agarose powder was added to 200 ml of DMEM with antibiotics, without serum. For dissolution, the medium was heated in a microwave until boiling 3 times. For sterilization, the solution was autoclaved. Autoclaved agarose solution was cooled to approximately 70°C and filtered with the help of a vacuum pump under sterile conditions. A small tube dispensing cassette after attaching to Combi Reagent Dispenser was washed with 70 % ethanol until there were no signs of any medium in the existing liquid. The cassette was washed with sterile PBS 3 times the volume inside the capillaries.

For each well of CellCarrier 384 well plate, 15 µl of agarose medium-high dispending speed was dispensed. Before adding the agarose solution to the wells, a certain volume must be passed through the capillaries until the drops drip evenly. The agarose plate should remain in the sterile box at room temperature for at least 20 minutes before seeding the cells to ensure even distribution and solidification of the agarose. For storage purposes, direct light should be avoided.

Because the plate was stored in a cold room, it was then left for 20 min in a sterile box to reach room temperature. The cells were plated in the amount of 15 000 in 50 µl per well with a multichannel pipette using a reverse pipetting technique to prevent bubble formation. If bubbles

form, it is necessary to destroy them with a sterile needle without damaging the agarose coating. For a co-culture experiment, cells were plated in proportion 4500 SH-SY5Y cells to 10500 SNB-75 cells to simulate better the natural conditions of the predominance of glial cells to neurons. For long-term experiments, all wells around the perimeter of the plate should be filled with PBS.

For imaging of spheroids for Feret's diameter measurement fluorescent microscope with a hundredfold magnification was used, and images were analyzed with ImageJ. For imaging of spheroids during seeding assay was used CellVoyager HC Imaging System used a 4× air objective.

4.5.6 Spheroids Differentiation

48 h after plating, half the old medium (25 µl) in each well was carefully aspirated. It is important to avoid damage to the spheroid or agarose coating and the formation of bubbles. For differentiation of SH-SY5Y, the complete medium was changed to the Differentiation Medium #1 or the Differentiation Medium #2. The concentration of differentiation reagents was doubled because only half of the final volume is added. After 72 h, half of the medium was changed to Differentiation Medium #3 or Differentiation Medium #4. The concentration of differentiation reagents was doubled. Cells can be maintained until the signs of decay appear, and the Differentiation Medium #3 and #4 were changed every 3-4 days.

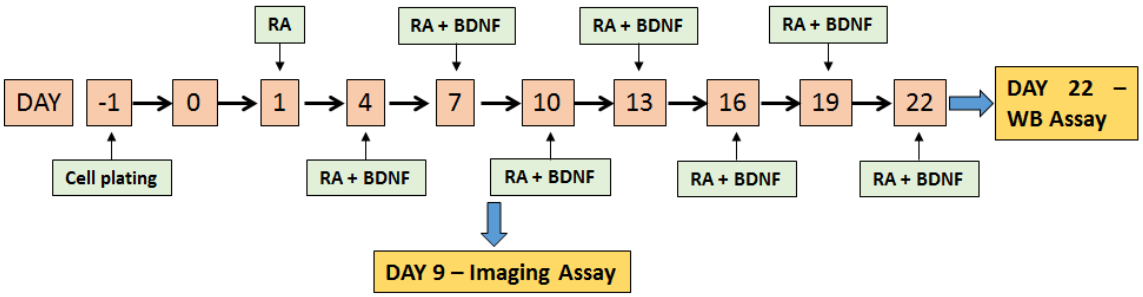

Figure 4.4: Spheroids monoculture differentiation protocol.

For the differentiation of co-culture, 48 h after plating half of an old medium was carefully changed to the Differentiation Medium #5, but the concentration was raised twice (NBM with 20 µM RA, 0.5 mM IBMX and 1 mM dibutyryl cAMP). After 72 h, half of an old medium was carefully aspirated. An old medium was changed to the Differentiation Medium #6. The concentration was doubled. Every 3-4 days, spheroid were imaged on a fluorescent microscope. After 9 days of differentiation, spheroids were collected for the Immunostaining and Imaging Assay. After 21-22 days of differentiation, spheroids were collected for the western blot assay.

4.5.7 Tau Aggregation Assay for Tau P301S Biosensor Cells, SH-SY5Y Monoculture and Co-culture with SNB-75 with TAU R3 Aggregates

For the tau aggregation assay, the following slightly modified protocol was used (Annadurai et al., 2022a). 160 µl of R3 aggregates (20 µM) were prepared. 128.2 µl of filtered PBS were mixed with 16 µl of aggregation buffer, 5.4 µl of heparin and 10,4 µl of monomers. The tube with the mixture was vortexed, covered with parafilm and put in the shaker for 48 h (37 °C, 1000 rpm).

For analysis with a fluorescent microscope, cells were plated on a CellCarrier/PhenoPlate 96-well plate (10000 cells, 100 µl of medium/well) and kept in an incubator (5 % CO_2 at 37°C) overnight. The transfection mixture was prepared using a Lipofectamine™ 3000 Transfection Reagent. R3 tau aggregates were diluted (100 nM final concentration) in Opti-MEM (5 µl/well for 2D culture in 96 well plates). R3 tau aggregates mixture with Opti-MEM were mixed with the Plus reagent (0.25 µl/well). LTX reagent was mixed with Opti-MEM (0.5 µL/well). Both mixtures were combined, vortexed and incubated for 15 min at room temperature. Then, a respective volume was added to the freshly changed growth medium in wells. The cells were incubated at 5 % CO_2/37°C for 72 hours.

For western blot analysis, cells were plated on a 6-well plate (0.5 mln cells/well, 2 ml medium/well) and kept in a 5 % CO_2 incubator at 37°C overnight. The transfection mixture was prepared with the same steps but 200 µl/well of Opti-MEM, 1.5 µl/well of Plus reagent and 3 5 µl/well of LTX were added instead of the amount that was mentioned above.

4.5.8 Fluorescent Microscopy and Image Analysis

Before imaging, nuclei were stained with 5 µM Hoechst 33342 dye. The previous medium was carefully aspirated and changed for Hoechst solution in complete DMEM. The cells were incubated for 10 min (37°C and 5 % CO_2), Hoechst solution was aspirated, cells were washed with 1x PBS, and complete DMEM was added. Imaging was performed 72 h after transfection on CellVoyager High-Content Imaging System (same conditions as in incubator) in a live-cell chamber with 60× objective. Images were analyzed by Columbus Image Data Storage and Analysis System (Columbus, ver. 2.9.1.699). Received data were processed in Microsoft Excel and GraphPad Prism (trial version).

4.5.9 Sample Collection for Western Blot

Before the start of the experiment, a box with ice was prepared. The collection of the samples started with the aspiration of a complete or differentiation medium (with floating cells). The medium was collected into separate 15 ml conical tubes for each of the conditions. Cells in the wells were washed with 1X PBS (at this step, cells start to detach and can be collected even without the addition of TrypLE). The cells with PBS were poured into the same tube and kept on ice to prevent protein degradation. If a certain number of cells remained attached to the surface, TrypLE (250-300 µl for 1 well of a 6-well plate) was added to support detachment, and the plate was incubated for 5 min (37°C). All the steps can be done in non-sterile conditions.

TrypLE was deactivated by the growth medium containing the serum, and the cell suspension was aspirated and poured into the same tube. The tubes were centrifuged at 1500

RPM for 5 min. The supernatant was carefully discarded, and the pellet resuspended in 1X PBS (1 ml), then transferred into a 1.5 mL microcentrifuge tube and centrifuged at 4 000 RPM for 5 min. The supernatant was discarded, and another 1 ml 1X PBS was added without disrupting the cells. The tubes were centrifuged as previously. The liquid was carefully aspirated and discarded first with a 1 ml pipette and then with a 100 ml pipette. The volume of residual liquid in the final sample was minimized to avoid the interference of impurities in further analysis. The samples were marked, processed, or stored in a –80°C freezer.

4.5.10 Sample Processing and Protein Concentration Measurement for the Detection of Insoluble Tau Fractions

The samples were kept on ice whenever it is possible. The centrifuge was turned on before the start of the procedure, set to a temperature of 4°C and left for 15 min. Lysis buffer (1x TBS + 0.05 % Triton X-100) was mixed with protease and phosphatase inhibitors according to the manufacturer's protocol before the experiment.

300 µL of the mixture was added to the samples. The pellets were resuspended with 1 ml pipettes. The mixture was incubated for 5 min on ice. Then samples were centrifuged at 500g and then 1000g for 5 min each at 4°C. The supernatant was transferred to the newly marked 1.5 mL microcentrifuge tubes (half of the volume can be stored in the freezer at -80°C as total fraction samples) and centrifuged at 15 000 RPM at 4°C for 1 h. The first pellet can be discarded.

After centrifugation ends, supernatant with Triton-soluble protein fraction was collected, and the newly formed pellet was washed with Triton lysis buffer 2 times and centrifuged at 15 000 RPM at 4°C for 1 min each time. The pellet was resuspended in 40-50 µL RIPA buffer previously mixed with proteinase and phosphatase inhibitors and sonicated for 1 min in a water bath sonicator at 50 % amplitude. It was preset on the 15-sec pulse on and 15-sec pulse off. The tubes were centrifuged at 12 000 RPM at 4°C for 30 minutes.

Supernatant with Triton-insoluble fraction was collected into new marked 1.5 mL microcentrifuge tubes, and both fractions were stored in a –80°C freezer. The protein concentration was determined for the total and soluble tau fractions. In the future, for electrophoresis and WB experiment, the volume of liquid-containing protein in a sample with an insoluble fraction should equal the sample containing a soluble fraction.

4.5.11 2D Sample Processing and Protein Concentration Measurement for the Detection and Semi-Quantitative Analysis of Biomarkers

50 µl of RIPA lysis buffer with inhibitors was added to the pellets with further resuspension. The samples were sonicated in a cold room for 1 min in a water bath (BRANSON sonicator) at 50 % amplitude. It was preset on the 15-sec pulse on and 15-sec pulse off. The tubes were centrifuged at 12 000 RPM at 4°C for 30 min. The supernatant was carefully collected without disturbance of the pellet to the new Eppendorf tubes, and the protein concentration was

measured using BCA assay in a 96-well plate. BCA reagent was prepared: 49 parts of reagent A were mixed with one part of reagent B.

10 µl of BSA standards (125, 250, 500, 750, 1000, 1500, 2000) was added (1 for each well). To the next 10 wells (blank measurements), 10 µl of RIPA lysis buffer was added. The maximum concentration that can be measured by BCA assay is 2 mg/ml. It is important to dilute the samples prior to the assay or use only 1 or 2 µl of the sample. 200 µl of BCA mixture was added to each well. The samples were incubated at 37°C for 30 min. Using a plate reader, the absorbance was measured on the Envision multimode plate reader (PerkinElmer) at 562 nm. Determination of the protein concentration was performed with the help of the calibration curve with standards and calculated in Microsoft Excel.

4.5.12 Sample Processing for Western Blot of Spheroids

Sample processing was performed as described above, but no centrifugation is needed until the addition of lysis buffer. The washing step in 1X PBS can be performed on a shaker.

4.5.13 SDS-PAGE Electrophoresis

SDS-polyacrylamide gels (1.5 mm thick, 10 % or 8 % depending on the molecular weight of the detectable protein) with 15 wells were prepared using the Bio-Rad Mini PROTEAN Tetra Cell system. Equal volumes of samples were mixed with 5X SDS gel loading dye (4 µl/well) after mixing with 10 % of β-mercaptoethanol. A lysis buffer was added to achieve an equal volume if the protein concentration was high. Mixtures were vortexed, centrifuged for 1-2 s and heated in a dry thermal block at 95°C for 5 min.

After cooling down, samples were loaded (20 µL of mixture/well) into the gel wells. Electrophoresis was run at 120 V for approximately 1.5 hours (for separation gels) and at 200 V for approximately 45 min (for gradient gels) until the dye hit the bottom of the cassette. 35 µg of proteins from each sample was used for western blot analysis if the amount of collected protein allowed.

4.5.14 Western Blot

Western blot was performed using Trans-Blot Turbo Transfer System – Ready-to-Assemble kit, following the BioRad kit's protocol for 1.5 mm gels transferring. Proteins were transferred onto a pre-activated nitrocellulose membrane (incubated for 2 min in a transfer buffer at room temperature). The sequence was as follows: a stack of paper, then a membrane, then gel and then a final stack of paper. After each step, the roller was used to remove the trapped air bubbles.

After transferring, the presence of the proteins was checked with Ponceau S Staining Solution and the membranes were washed 3-4 times with dd water. The membranes were blocked in 5 % BSA in TBST buffer for 1 h at room temperature while shaking at the 3rd speed. The membranes were incubated with primary antibodies (1:1000 diluted in 5 % BSA in TBST

buffer) overnight in a cold room (4°C). The next day the membranes were washed in TBST buffer 3 times (15 min each).

The membranes were incubated in respective secondary anti-goat, anti-mouse, anti-rabbit or anti-sheep secondary antibodies conjugated with Alexa Fluor or HRP fluorescent dye for 1 h at room temperature on a shaker protected from direct light. The membranes were washed with TBST buffer 4 times (10 min each). After the last wash, the membranes were imaged in the Bio-Rad Gel Documentation system. For measuring band intensity, ImageJ was used with the following sequence of actions: Image – Type – 8-Bit. Then: Analyze - Set Measurements – Highlight Area, Min & max grey value and Integrated density. Next, the integrated intensity of the bands was measured, followed by subtraction of the blank. Next, the normalization of GAPDH was performed. Calculations were made using Microsoft Excel 2016.

The membranes were incubated in GAPDH primary antibodies solution for 1 h at room temperature on a shaker protected from direct light and washed with TBST buffer 4 times (10 min each). The membranes were incubated in Donkey anti-Mouse IgG (H+L Secondary Antibody, Alexa Fluor™ 488 (1:2000) for 1 h, washed 4 times with TBST buffer and imaged in the Bio-Rad as described above.

4.5.15 Spheroid Immunochemistry

Spheroids (6-10 from each experimental condition) were carefully collected into 15 ml tubes with a 1 ml mechanical pipette. The medium was aspirated, spheroids were washed with 1x PBS, transferred to 1.5 ml Eppendorf tubes, and washed 2 times with 1x PBS. The spheroid structures were fixed in the fixation buffer (rotating on SB3 for 2 h at room temperature and covered with tin foil to protect it from direct light). After fixations, spheroids were carefully collected from the cap and walls of the tube if they are stuck and washed 3 times for 15-20 min at room temperature. All the manipulations were with nitrile gloves.

Spheroids were permeabilized in a permeabilization buffer (rotating on SB3 for 2 h at room temperature and covered with tin foil to protect it from direct light). They were carefully collected from the cap and walls of the tube if spheroids are stuck and blocked in the blocking mixture (300 µl per tube) for 2 h under the conditions described above. Then spheroids were incubated in 250 µl of primary antibodies (MAP2 1:400 in buffer #2 + 5 % DMSO + 3 % DS + 3 % GSA/ β3-tubulin 1:500 in buffer #2 + 5 % DMSO + 3 % DSA + 3 % GSA) for 2 h under the conditions described above. Spheroids were washed in buffer #2 3 times (20 min each).

As the next step, spheroids were incubated in 250 µl of secondary antibodies (For MAP2 Goat anti-Rabbit IgG (H+L) Cross-Adsorbed Secondary Antibody, Alexa Fluor™ 647 1:500 in buffer #2 + 5 % DMSO + 3% DSA + 3 % GSA/For β3-tubulin 1:500 in buffer #2 + 5 % DMSO + 3 % DS + 3 % GSA) for 2 h as before. Then they were stained for 1 h with freshly prepared Hoechst 33342 dye (10 µM diluted in buffer #2), avoiding direct light. Spheroids were washed in buffer #2 3 times (30 min each).

The immunostaining process can be interrupted for 1-2 days after completing steps 1 and 2, but steps 3 – 5 were finished in 1 day. Spheroids were kept in a cold room protected from light.

Spheroids were imaged using the Confocal microscope Carl Zeiss LSM 780. At least 2 randomly selected organoids were imaged for each experiment.

5. RESULTS

5.1 SH-SY5Y Cells Change the Morphology Closer to Mature Neurons After RA and BDNF Treatment in 2D Culture

More nodes and branching neurites under the differentiation condition can be observed, which is typical for mature neurons (Figure 5.1A). The data are consistent with those described in the literature (Agholme et al., 2010). Cells cultured in NBM without additional differentiation factors also show morphological features of mature neurons. It can be explained by the lack of serum in the growth medium and the presence of insulin in the B-27 supplement (Martin et al., 2022). When SH-SY5Y cells are grown in complete DMEM, overgrowth is observed from days 4-5, making the analysis impossible. When cells are grown in NBM without adding RA and BDNF, there are areas of low cell density with longer processes and areas where the cells are crowded so tightly that it becomes impossible to separate individual processes and analyze them. This makes it difficult to compare the SH-SY5Y morphology of the pure NBM condition with the differentiated cell condition.

In addition to the shorter neurites of non-differentiated cells, which are depicted in Figure 5.1., it is also possible to see the predominate distribution of MAP2 into soma under undifferentiated conditions and a more uniform distribution of MAP2 between neurite and soma in differentiated neuronal-like SH-SY5Y cells (highlighted with yellow arrows).

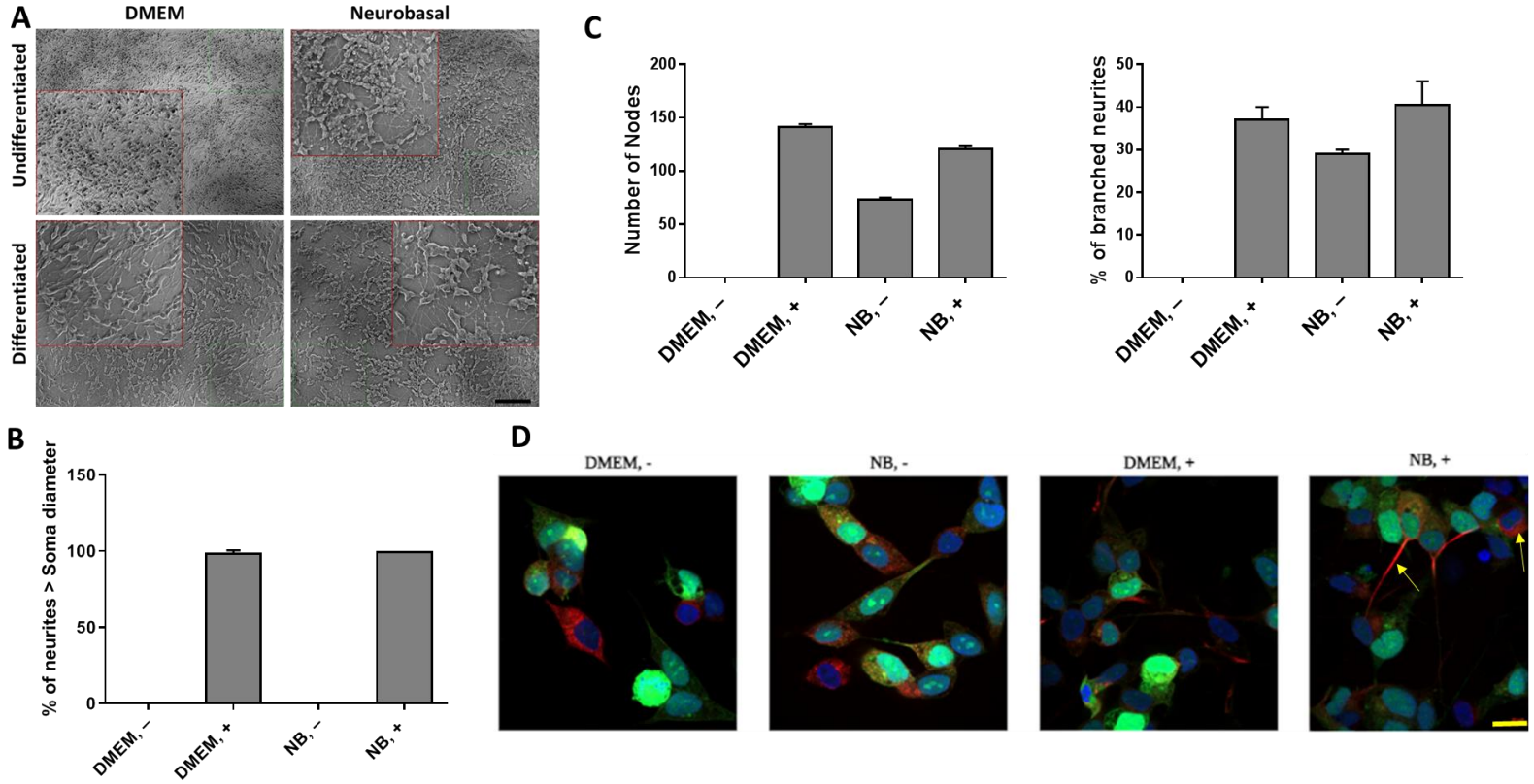

Figure 5.1: A) Comparison of the morphology of undifferentiated SH-SY5Y cells in complete DMEM (–) and Neurobasal medium (NB, –) vs differentiated SH-SY5Y cells differentiation in the medium #3 (DMEM, +) and #4 (NB, +). The area of the image (highlighted in green) is enlarged by 2 times (highlighted in red). Scale bar is in the lower right corner (200 µm). **B)** Comparison of ratios of neurite length and soma diameter of undifferentiated SH-SY5Y cells in DMEM, – and NB, – vs SH-SY5Y cells after differentiation (DMEM, + and NB, +). Data are mean ± SEM, n =3. **C)** The number of nodes (the left graph) and the percentage of branching neurites (the right graph). **D)** Comparison of the morphology of undifferentiated vs differentiated SH-SY5Y cells. Expression of MAP2 is highlighted in red, and tau (a double mutant with GFP) is highlighted in green. Cell nuclei are stained blue with Hoechst 33342. Data are mean ± SEM, n = 3. Yellow scale bar is in the lower right corner (20 µm).

5.2 SH-SY5Y Cells Express Biomarkers Specific to Mature Neurons after RA and BDNF Treatment in 2D Culture

Figures 5.4 and 5.5 show that differentiation of neuroblastoma in NB significantly increases the levels of ChAT expression in SH-SY5Y cells expressing P301L, and the cells change to a more cholinergic type of neuron. The data are consistent with those described in the literature (de Medeiros et al., 2019).

The absence of VGLUT 1 bands conflicts with previous findings in the literature (Martin et al., 2022). Other studies suggest the possibility of neuroblastoma differentiation proceeding along the path of transformation into neuron-like cells similar to glutamatergic or cholinergic neurons under almost similar differentiation conditions (Bell and Zempel, 2022).

From western blots shown in Figures 5.6 and 5.7, it can be concluded that as a result of the differentiation of SH-SY5Y in NB, the levels of expression of MAP2 C/D and β-III-tubulin increased significantly in the parental SH-SY5Y cell line. This is another evidence in favor of neuroblastoma differentiation into neuron-like cells.

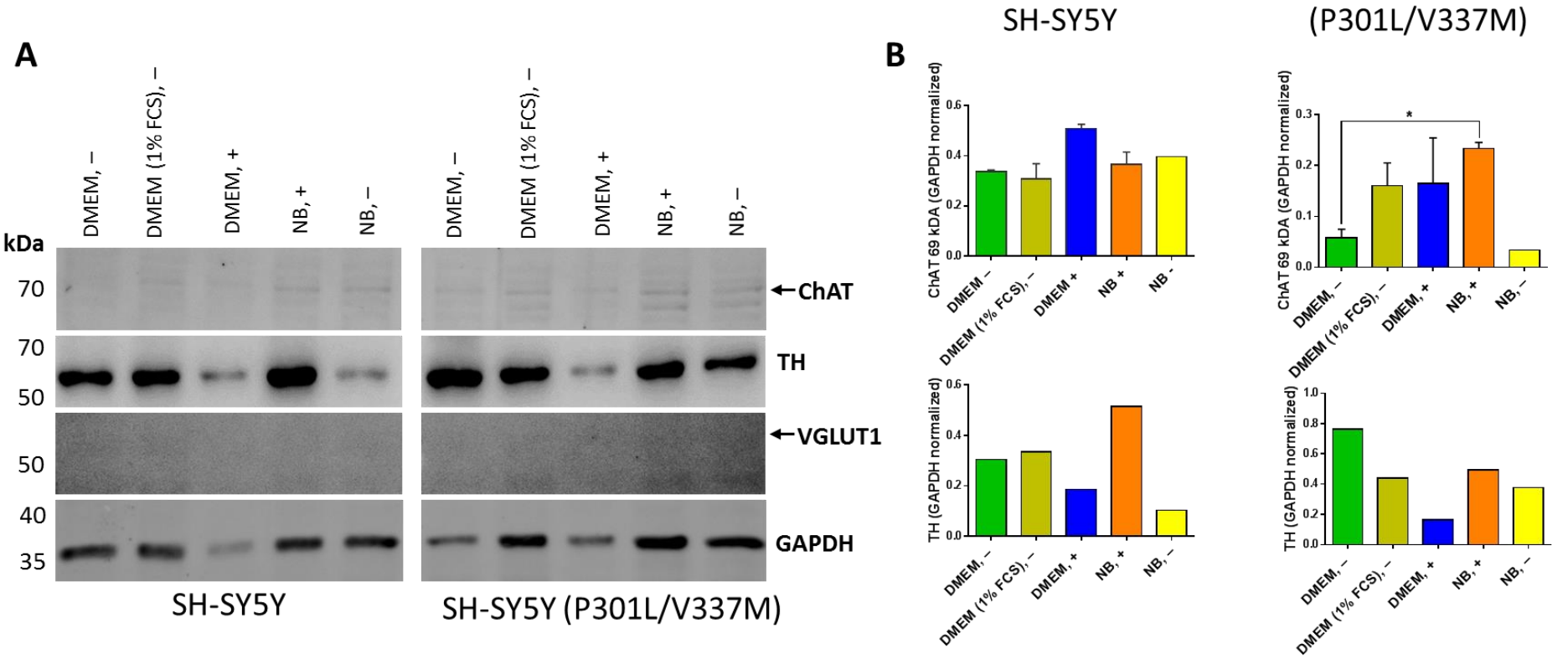

Figure 5.2: **A)** Comparison of expression levels of choline acetyltransferase (ChAT), tyrosine hydroxylase (TH), vesicular glutamate transporter 1 (VGLUT1) in differentiated and undifferentiated SH-SY5Y cells grown in complete DMEM (DMEM, –) and NBM (NB, –) vs SH-SY5Y cells after differentiation in medium #3 (DMEM, +) and #4 (NB, +). **B)** Quantification of ChAT and TH expression in undifferentiated SH-SY5Y cells in complete DMEM (DMEM, –) and NBM (NB, –) vs SH-SY5Y cells after differentiation in medium #3 (DMEM, +) and #4 (NB, +). +). Parental cells were compared to cells transduced with Tau.K18(P301L/V337M). Data are mean ± SEM, n = 2.

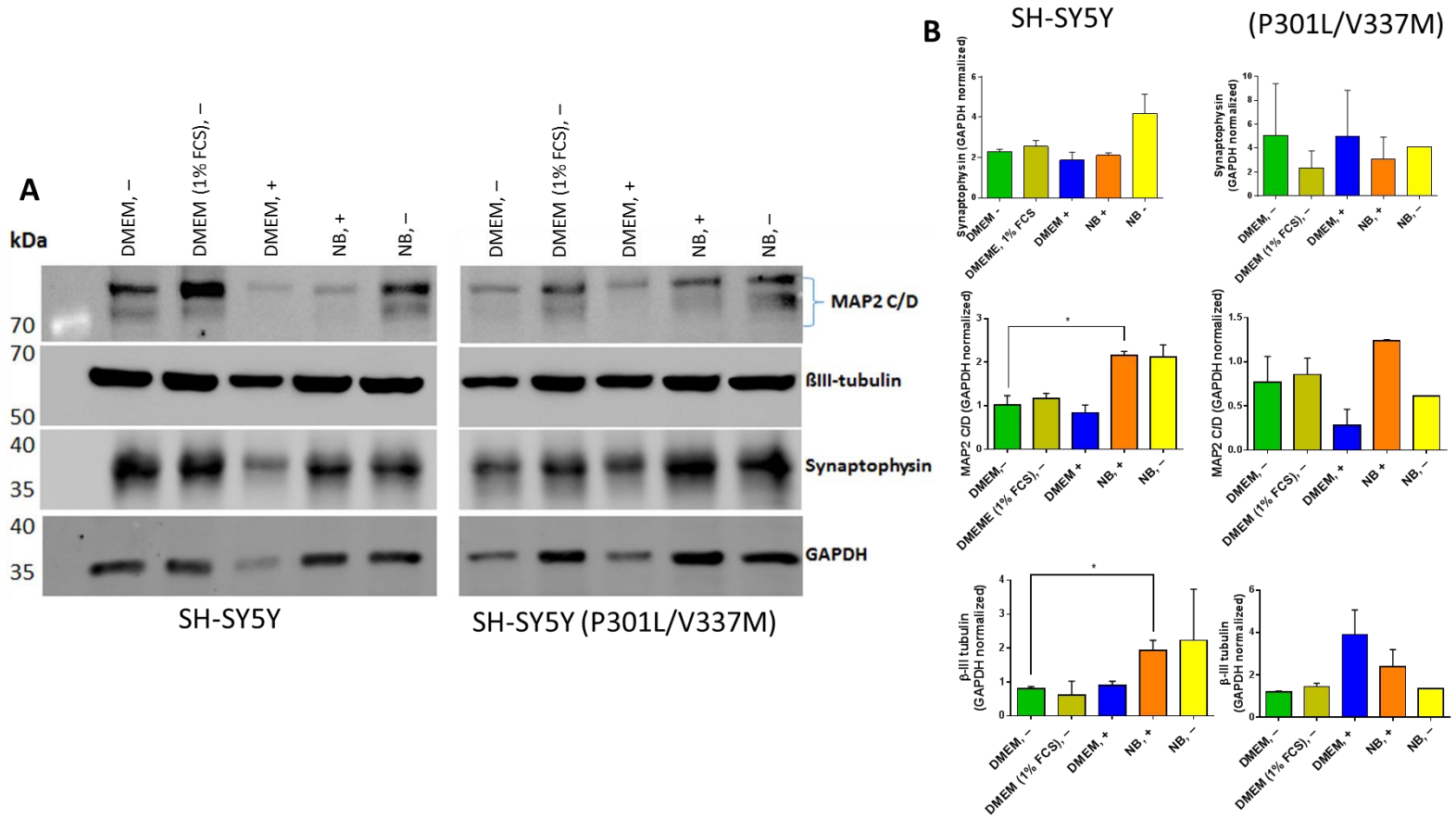

Figure 5.3: **A)** Comparison of the biomarkers levels of expression of undifferentiated SH-SY5Y cells in complete DMEM (DMEM, –) and NBM (NB, –) vs SH-SY5Y cells after differentiation in medium #3 (DMEM, +) and #4 (NB, +). Parental cells were compared with cells after lentiviral transduction (P301L – mutated 2N4R form of tau). **B)** Quantification of expression levels proteins in undifferentiated SH-SY5Y cells in complete vs in SH-SY5Y cells after differentiation in medium #1 and #3 (DMEM, +) and #2 and #4 (NB, +). Parental cells were compared to cells transduced with lentiviral vectors containing Tau.K18(P301L/V337M). Data are mean ± SEM, n =2.

5.3 SH-SY5Y Cells Express at Least 5 Tau Isoforms Specific for Mature Neurons Without Treatment and after RA and BDNF Treatment in 2D Culture

The experiment demonstrated the presence of at least 5 tau isoforms in parental SH-SY5Y cells and 6 forms in genetically-modified cells (The single line band is approximately located at 45 +/- 2 kDa). The parental cells were compared to those transduced with lentiviral vectors containing Tau.K18(P301L/V337M).

Expression was observed even in undifferentiated cell-line. For a significant confirmation of the results of the experiment, the use of positive control (a sample containing protein from an adult human brain or tau isoforms ladder) is recommended. A special gradient gel is required to separate 0N4R (39,7 kDa) and 1N3R (40 kDa).

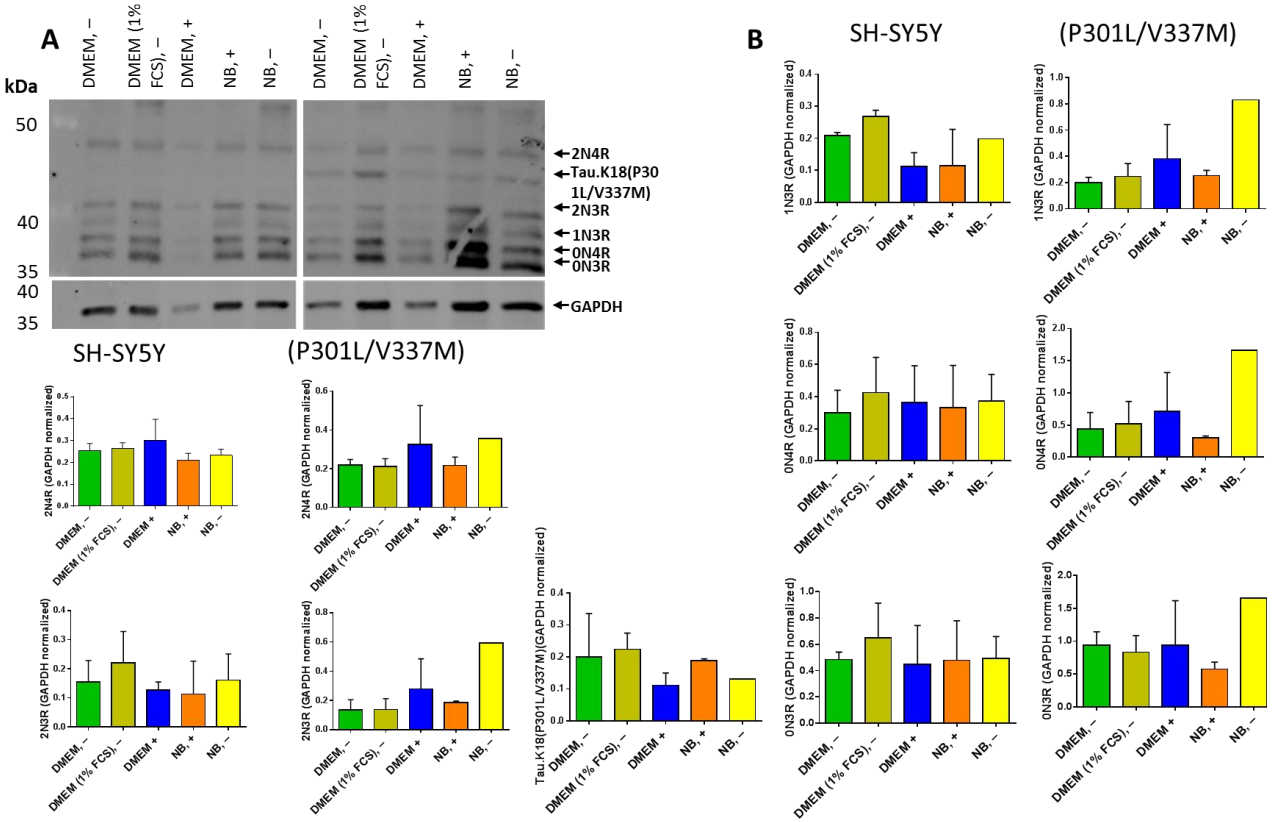

Figure 5.4: **A)** Comparison of tau isoforms expression in undifferentiated SH-SY5Y cells in complete DMEM (DMEM, –) and NBM (NB, –) vs. in SH-SY5Y cells after differentiation in medium #3 (DMEM, +) and #4 (NB, +). Parental cells were compared to cells transduced with Tau.K18(P301L/V337M) modified by lentiviral vectors. B**)** Quantification of expression levels of native tau isoforms in undifferentiated SH-SY5Y cells in complete DMEM (DMEM, –) and NBM (NB, –) vs. SH-SY5Y cells after differentiation in medium #3 (DMEM, +) and #4 (NB, +). Parental cells were compared to cells transduced with lentiviral vectors containing Tau.K18(P301L/V337M). Data are mean ± SEM, n =2.

5.4 SNB-75 cells express biomarkers specific for mature astrocytes without treatment and dibutyryl cAMP and IBMX treatment in 2D culture

SNB-75 cells were modified with DsRed, Plenti-CMV-MCS-RFP-SV-puro (Plasmid #109377, Addgene) according to the procedure described in chapter 4.5.2 and treated according to the method described in chapter 4.5.4. Representative images show the difference in the shape of undifferentiated and differentiated SNB-75 in mono- and co-culture. Undifferentiated cells are characterized by an elongated shape, making it difficult to separate the processes from the body visually. Differentiated SNB-75 cells are similar to astrocytes (highlighted with red arrows below) in shape and the presence of at least five processes, some of which are divided into separate branches (Figure 5.5.A).

Figures 5.12 and 5.13 show an apparent upregulation of GFAP expression in SNB-75 cells after differentiation. However, no significant difference in expression level was found. This data suggest that the differentiation protocol induced adult human astrocyte-like characteristics in SNB-75 cells.

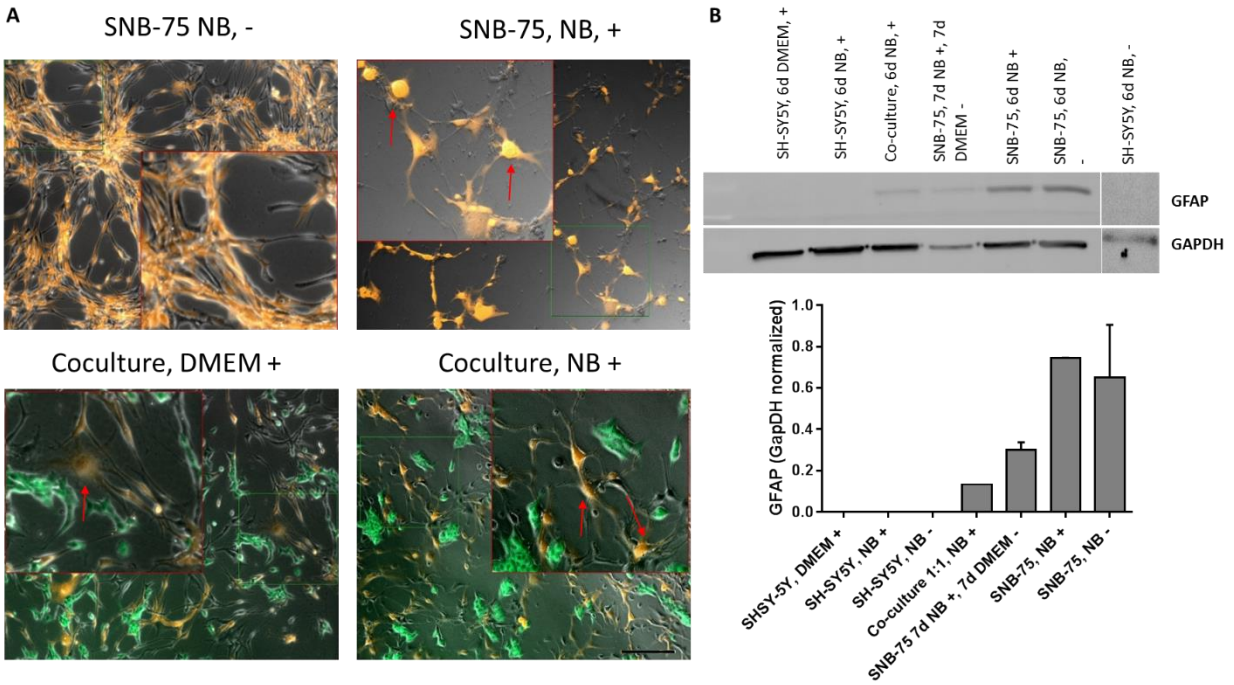

Figure 5.5: **A)** Comparison of the morphology of undifferentiated and differentiated SNB-75 cells in DMEM and undifferentiated and differentiated co-cultures (SH-SY5Y and SNB-75 cells at a ratio of 3:7 in DMEM and NBM). The area of the image (highlighted in green) was enlarged by 2 times (highlighted in red). Scale bar is in the lower right corner (200 µm). **B)** Western blot showing GFAP expression in monocultures and cocultures. Lane 1 – protein marker; Lane 2 & 3 – SH-SY5Y cells after differentiation in DMEM + and NBM + for 6 days; Lane 4 – Co-culture of SH-SY5Y and SNB-75 cells after differentiation in NB for 6 days; Lane 5 – Monoculture of SN-75 cells differentiated in NB for 7 days and then cultured in complete DMEM media for 7 days; Lane 6 – SNB-75 cells differentiated for 7 days in NB media; Lane 7 – Undifferentiated SNB-75 cells cultures in NB media; Lane 8 – Undifferentiated SH-SY5Y

cells in NBM. Data are mean ± SEM, n =2. 5.5 3D cultures of SH-SY5Y cells and SH-SY5Y/SNB-75 and after RA and BDNF treatment.

5.5 3D cultures of SH-SY5Y and SH-SY5Y/SNB-75 and after RA and BDNF treatment

Spheroids were formed according to the procedure described in chapter 4.5.5 after both SH-SY5Y and SNB-75 cell lines were transduced with lentiviral particles. Because the form of spheroids differs from the ideal sphere, the Feret diameter function was used (ImageJ) to improve the accuracy. The measurements were carried out on two batches of spheroids. Of each, 4-5 spheroids were randomly selected for measurements.

The spheroids growing in the complete medium (both DMEM and Neurobasal) began to fall apart after 16 days, so they were collected for the western blot on day 17 when the last images were also taken. Based on the result of the spheroids measurement (Figure 5.6), their continuous growth can be observed. It can be caused by a heterogeneous population of the parental cells (S- and N-type of SH-SY5Y culture, which show different responses to treatment). It can also be explained by the difficulty of entering the centre of the spheroid for macromolecules such as BDNF (molecular weight is approximately 28 kDa).

From Figure 5.7, it can be concluded that SH-SY5Y cells and SH-SY5Y/SNB-75 cells grow in co-culture conditions and express biomarkers specific for the mature neurons after RA and BDNF treatment in 3D culture. They also form tighter nodes throughout the neurites. The samples for western blot experiments were collected after 22 days of differentiation in mono- and co-culture in NBM and DMEM. The spheroids for imaging were collected after 9 days of differentiation.

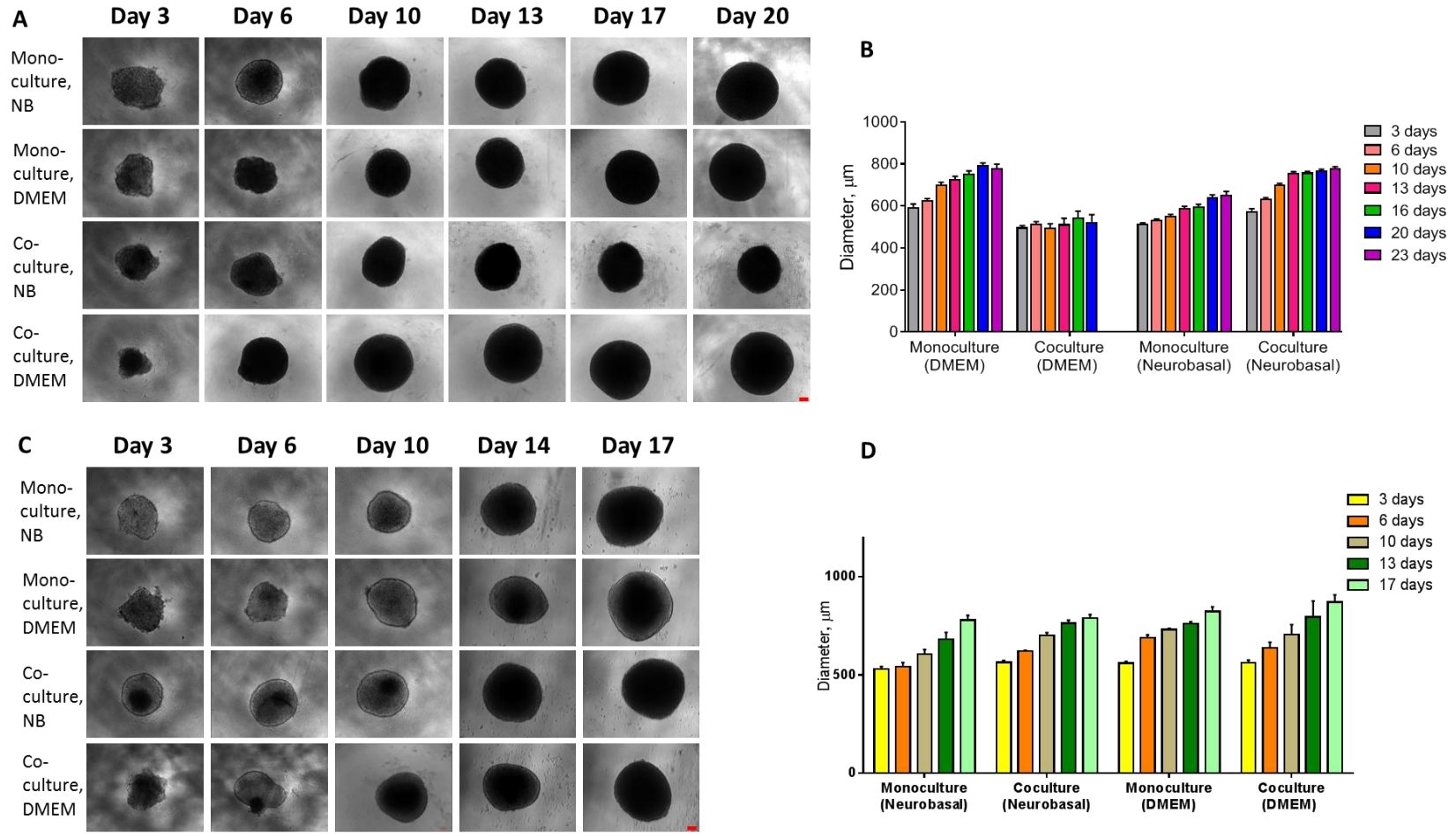

Figure 5.6: Images of monoculture and coculture 3D spheroids under different differentiation conditions. The scale bar in red (100 µm) is in the bottom right corner. **B)** Changes in the Feret diameter of spheroids over time upon growth under differentiation conditions. Data are mean ± SEM, n =2. **C)** Images of monoculture and coculture 3D spheroids growing in complete media without differentiating factors. The scale bar in red (100 µm) is in the bottom right corner. **D)** Changes in the Feret diameter of spheroids over time grow in complete media. Data are mean ± SEM, n =2.

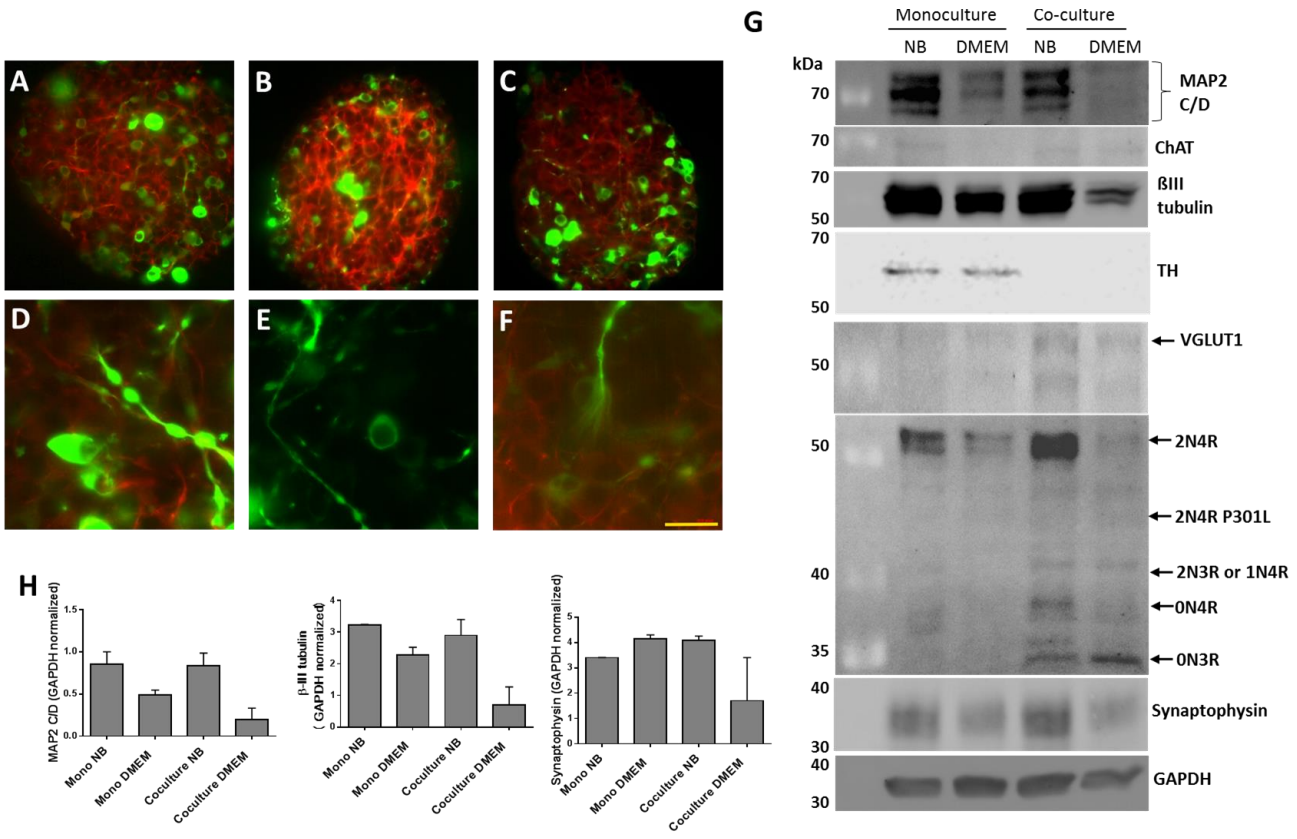

Figure 5.7: **A)** Monoculture SH-SY5Y in DMEM, Day 9 of differentiation. **B)** Monoculture SH-SY5Y in NBM, Day 9 of differentiation. **C)** Co-culture SH-SY5Y:SNB-75 (3:7) in NBM. **D)** Neurite with nodes with GFP-Tau (Monoculture SH-SY5Y in DMEM). **E)** Neurite with nodes with GFP-Tau (Monoculture SH-SY5Y in NBM). **F)** Neurite with nodes with GFP-Tau (Co-culture SH-SY5Y:SNB-75 (3:7) in NBM). Yellow scale bar is in the lower right corner (20 µm). Note the clear GFP-tau signal in nodes and soma. **H)** Comparison of expression levels of MAP2 C/D, synaptophysin and βIII-tubulin in monoculture spheroids of SH-SY5Y cells and co-cultures spheroids of SH-SY5Y and SNB-75 cells growing at a ratio of 3:7 after 22 days of differentiation in NBM and DMEM. **G)** Comparison of the expression levels of βIII-tubulin, synaptophysin, MAP2 C/D, and tau isoforms after western blot measurement. Data are mean ± SEM, n =2.

5.6 Exogenous R3 aggregates induced intracellular aggregation in Tau RD P301S FRET Biosensor cells and co-culture of BS with SNB-75

Tau RD P301S FRET Biosensor cells were plated with a concentration of 10,000 cells per well in the case of a monoculture and a mixture of 3,000 biosensor cells with 7,000 SNB-75 cells to form a coculture. Additional experiments were carried out with a coculture in which SNB-75 cells were transplanted to TAU biosensor cells 24 hours after transfection with R3 fibrils at a concentration of 100 nM according to the protocol described in chapter 4.5.8. so that the percentage of insoluble tau seeds formed relative to the total number of cells can be calculated. Figure 5.8 shows the nuclei of pathological tau aggregates in TAU BS cells. At the same time, not a single reliable case of penetration of tau seeds into SNB-75 cells was found. No significant effect of astrocyte-like cells on tau seeding was found during the experiment.

It should be noted that experiments with TAU biosensor cells suffer from a lack of calculation accuracy because they grow at different rates and several times faster than SNB-75. In addition, they tend to grow in 2 layers, which can lead to the concealment of part of the pathological seeds from the measurement with the instrument.

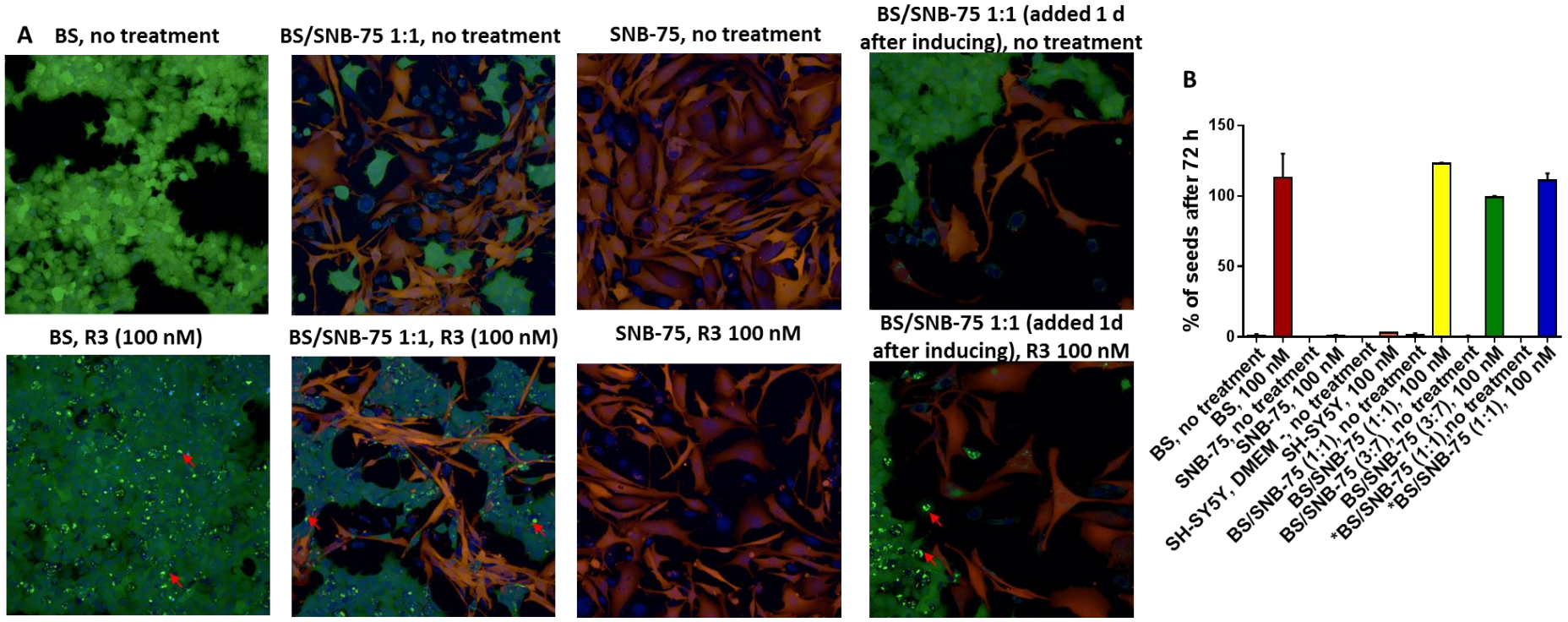

Figure 5.8: **A)** Induction of intracellular tau aggregation after transfection with R3 (100 nM) fibrils after 72 h. Red arrows mark intracellular aggregates. 20x objective. **B)** An asterisk indicates a coculture in which SNB-75 cells were transplanted to TAU biosensor cells a day after transfection with R3 fibrils at a concentration of 100 nM. "DMEM -" indicates no differentiation agents were added to the cell culture medium. Data are mean ± SEM, n =2.

5.7 Exogenous R3 aggregates induced intracellular aggregation in undifferentiated SH-SY5Y cell line and co-culture of SH-SY5Y with SNB-75 (ratio 3:7)

Figure 5.9 shows that neuroblastoma cells can form tau aggregates after transfection with R3 fibrils at a concentration of 100 nM. The efficiency of this process is less than in Tau RD P301S FRET Biosensor cells. This problem can be partly solved by sorting by selecting cells with a high proportion of tau-GFP expression on a flow cytometer.

In contrast to Tau RD P301S FRET Biosensor cells, SH-SY5Y in coculture with SNB-75 at a ratio of 3:7 showed a decrease in the seeding efficiency and spread of pathological forms of tau after transfection with R3 fibrils at a concentration of 100 nM 72 hours after transfection with Lipofectamine 3000.

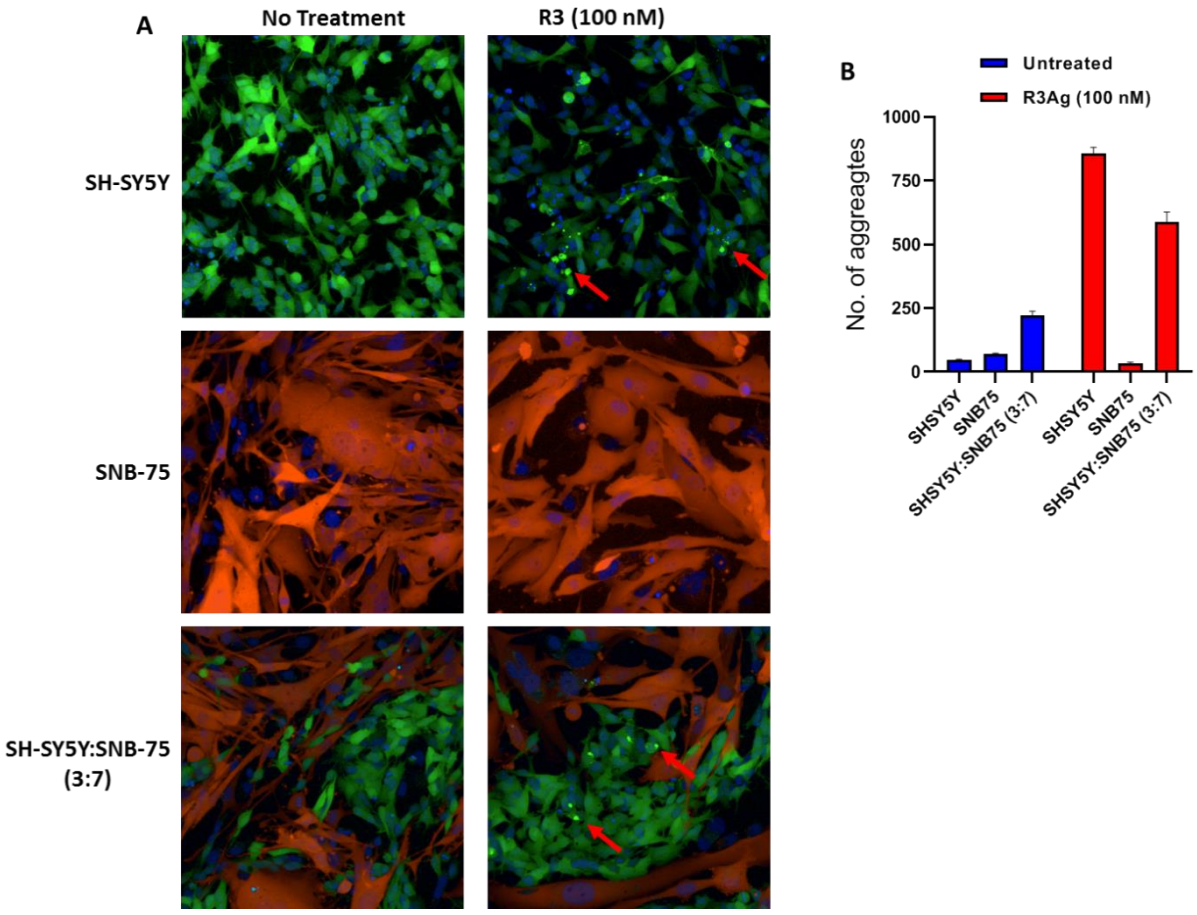

Figure 5.9: **A)** Induction of intracellular tau aggregation after transfection with R3 (100 nM) fibrils (72 h). Co-culture SH-SY5Y:SNB-75 (3:7) grew in DMEM with 10% FCS. Red arrows marks intracellular aggregates. During the experiment, a lens with a magnification of 20X was used. **B)** Results of absolute counts of tau aggregates in undifferentiated monoculture of SH-SY5Y cells and coculture of SH-SY5Y:SNB-75 (3:7). Data are mean ± SEM, n =2.

5.8 Exogenous R3 aggregates induced intracellular aggregation in Tau RD P301S FRET Biosensor cells (BS) in mono- and coculture (ratio BS:SNB-75 = 3:7) and differentiated SH-SY5Y cell line and differentiated co-culture of SH-SY5Y with SNB-75 in 3D (ratio SH-SY5Y:SNB-75 = 3:7)

The SH-SY5Y spheroids were planted according to the protocol described in chapter 4.5.5 and differentiated according to the protocol from chapter 4.5.6. After 9 days of differentiation, transfection with R3 fibrils was performed at a concentration of 100 nM. Spheroids were aspirated with a 1 ml pipette from an agarose plate and transferred to a 384-well plate for imaging.

Tau RD P301S FRET Biosensor cells spheroids were seeded in 384 well plates at concentration 10 000 cells per well. Three thousand Tau RD P301S FRET Biosensor cells were mixed with 7000 SNB-75 cells to generate cocultures. Transfection with R3 fibrils at a concentration of 100 nM was carried out using Lipofectamine 3000 5 days after the start of spheroid formation. After 72 hours, imaging was carried out on the CellVoyager 7000 following the protocol described above.

In Figure 5.10, yellow arrows mark places of formation of tau aggregates insoluble in physiological conditions. Unfortunately, CellVoyager could not provide an accurate count of the aggregates, but only to provide images for qualitative analysis and material for demonstration.

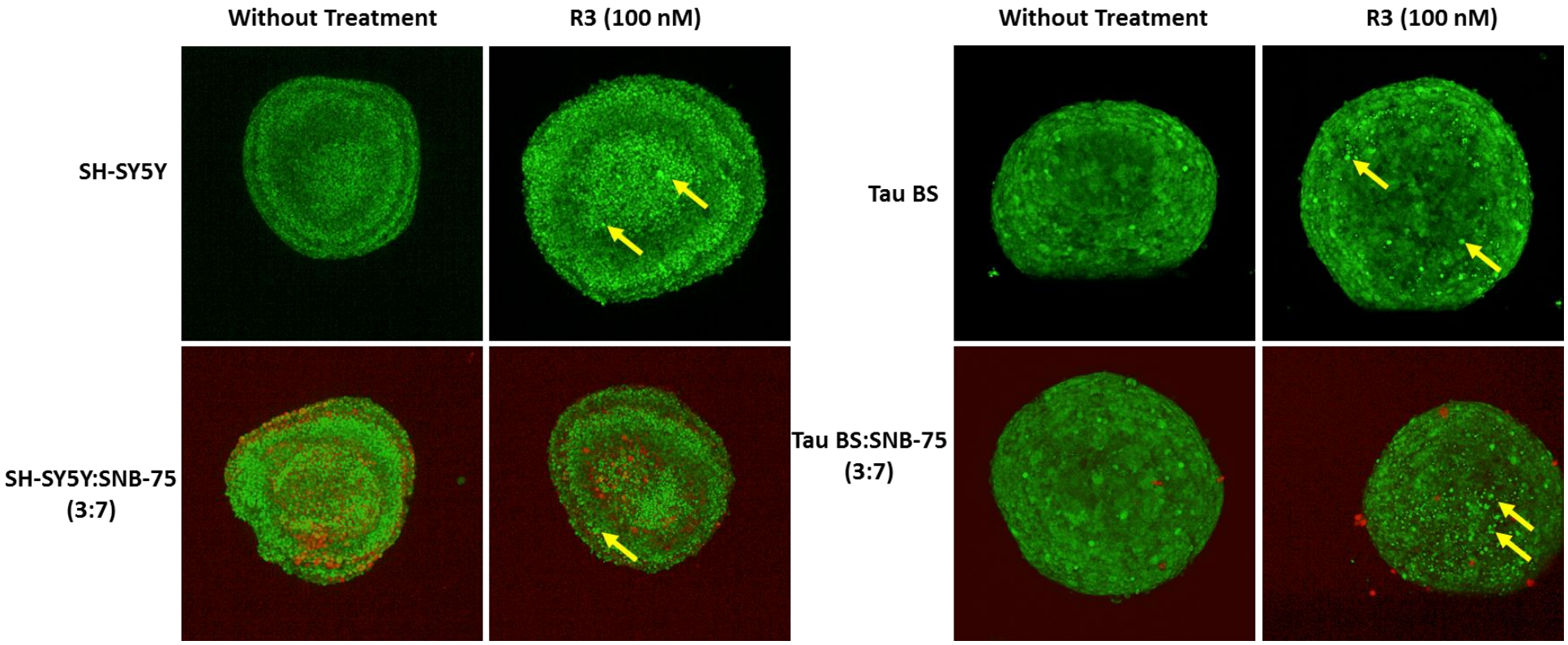

Figure 5.10: Figure 5.10 Induction of intracellular tau aggregation in Tau RD P301S FRET Biosensor cells and SH-SY5Y under different conditions after transfection with R3 (100 nM) fibrils after 72 h Induction of intracellular tau aggregation in spheroids in mono- and coculture after transfection with R3 (100 nM) fibrils (72 h). Yellow arrows indicate intracellular aggregates. During the experiment, a lens with a magnification of 20X was used.

6. DISCUSSION

During this master thesis work, an attempt was made to compare the formation of tau aggregates under conditions of differentiated and undifferentiated cells. To approximate the conditions to physiological ones, it was chosen to form spheroids with SH-SY5Y made in coculture with astrocyte-like cells. The choice of the cell line is explained by the popularity of this type of cell in experiments, cytotoxicity studies, modeling the development of Parkinson's and Alzheimer's diseases. It provides data for the possibility of comparing and changing cell differentiation conditions and their transfection. Protocols are also known for differentiating a cell line into cells similar to adult acetylcholinergic, glutamatergic and dopaminergic neurons or neuron-like elements that express a mixed type of biomarkers. (Agholme et al., 2010; Bell and Zempel, 2022)

Experiments on various methods of differentiation were carried out with the following goals:

1. Slow down or completely stop the process of cell division to minimize the influence of the growth of their number on the calculation of the efficiency of tau seeding.
2. To avoid the unknown influence of cytoskeletal proteins of immature neurons (for example, GFAP) and enzymatic cascades typical for different cell cycle phases.
3. To track simultaneously other important for long-term memory formation cytoskeletal proteins in neurites (β-III tubulin or MAP2) and the degradation of processes over time.
4. To reduce the cost of conducting experiments without losing the intensity of expression of biomarkers of interest.

Prior to transfection experiments, SH-SY5Y cells were modified with Tau.K18(P301L/V337M) (Addgene) to facilitate the confirmation of the formation of aggregates with tau-fuse GFP and the possibility of conducting a quantitative analysis with a larger sample. SNB-75 cells were transduced with DsRed, Plenti-CMV-MCS-RFP-SV-puro (Addgene) to facilitate their visual identification and selection in cocultures. The difference in expression between transduced Tau.K18(P301L/V337M), pMK1253 GFP-associated neuroblastoma cells was observed under fluorescent and confocal microscopes (Figures 5.5, 5.7). The influence of the transduction and expression irregularity of GFP of the clear tau can also be observed in Figure 5.4 at a level of approximately 45 kDa (GAPDH plot of the normalized GFP associated with Tau.K18(P301L/V337M). When imaging on the CellVoyager 7000 (Figures 5.9, 5.10), this could also complicate the recognition of forming aggregates, since the analysis is based on comparing the luminescence level in the green spectrum in the BP525/50 channel with the selected GFP fluorophore.

Cells were transfected with Lipofectamine 3000 with R3 tau fibrils capable of forming insoluble forms of tau in infected cells. The studies were conducted following the procedure outlined in Figure 4.2 in Chapter 4.5.4 while neuroblastoma cells were growing in a monolayer before and after adding differentiation agents.

The concentration of R3 fibrils (100 nm) and the time given for the spread of pathological seeds were chosen to be the same for all conditions. Quantitative comparison with transfected

spheroids was not possible at this stage of the study. The choice of the cell line for tau seeding control was made based on an article that proposes a method for carrying out tau seeding in vitro with a known rate of propagation of pathological forms of tau protein (Annadurai et al., 2023).

SNB-75 cells also demonstrated the ability to influence tau seeding. However, it is impossible to draw strict conclusions without the prior arrest of cell division. The desynchronization of cell cycles and the high rate of division of neuroblastoma compared to the glioma cell line complicate the analysis of the obtained information. For further research, it will be necessary to experiment with terminal differentiated mono- and co-culture. The cells should be pre-coated with poly-D-lysine 96-well plates for long-term imaging.

7. CONCLUSION

In conclusion, a reliable system for modeling tau seeding in neuron-like SH-SY5Y growing in coculture with astrocytes was established in this thesis. However, in the course of the experiments:

1) a differentiation protocol was validated for SH-SY5Y cells which let differentiate neuroblastoma into cells close in phenotype to mature acetylcholinergic neurons;
2) a protocol was found for the differentiation of SNB-75 cells, which had not been found before in the literature;
3) conditions were found for maintaining neuron-like and astrocyte-like cells in the condition of spheroids in coculture;
4) the possibility of the formation of aggregates in undifferentiated and differentiated SH-SY5Y cells in 2D and 3D was confirmed;
5) the possibility of quantitative analysis for studying tau seeding in SH-SY5Y cells in the monolayer was confirmed. So far, only a qualitative demonstration of the presence of seeds of insoluble tau has been found for spheroids.

To improve the results and complete the work on the model, it is important to

- In order to obtain cells with homogeneous expression of the GFP-fused tau protein, flow cytometry cell sorting must be performed.
- In addition to GFAP antibodies, to confirm the differentiation of SNB-75 cells, it would be possible to use antibodies to CD44 and to aquaporin 4, which are biomarkers for astrocytes from different areas of the brain.
- Due to non-specific bands on membranes after incubation in polyclonal antibodies, it is possible to improve the measurement accuracy by using monoclonal antibodies.
- In order to unify and improve the accuracy of semi-quantitative measurement of the intensity of the bands, it will be important in the future to use only one type of membrane (nitrocellulose or PVDF).
- Monitor the protein concentration in the samples using a different technique. A special gradient gel is required to separate 0N4R (39.7 kDa) and 1N3R (40 kDa).

- For a significant confirmation of the experiment's results, positive control (a sample containing protein from an adult human brain or tau isoforms ladder) is recommended.
- For further research, it will be necessary to experiment with terminal differentiated mono- and co-culture. The cells should be pre-coated with poly-D-lysine 96-well plates for long-term imaging to avoid detachment and death of differentiated cells during medium change or staining.

The findings described in this thesis shed some light on the differences in the induction of endogenous tau aggregates in the SH-SY5Y cells and coculture with SNB-75 astrocyte-like cells after transfection by exogenous R3 fibrils, hopefully facilitating further research on this topic. It also shows the necessity to develop or modify a reliable method for calculating tau aggregates in spheroids. As an example, methods such as confocal microscopy or lightsheet microscopy with immunostaining can be taken into account as a perspective (Batenburg et al., 2023; Seidel et al., 2012)

REFERENCES

Agholme, L., Lindström, T., Kågedal, K., Marcusson, J., Hallbeck, M., 2010. An in vitro model for neuroscience: differentiation of SH-SY5Y cells into cells with morphological and biochemical characteristics of mature neurons. J Alzheimers Dis 20, 1069–1082. https://doi.org/10.3233/JAD-2010-091363

Ahmed, T., Van der Jeugd, A., Blum, D., Galas, M.-C., D'Hooge, R., Buee, L., Balschun, D., 2014. Cognition and hippocampal synaptic plasticity in mice with a homozygous tau deletion. Neurobiology of Aging 35, 2474–2478. https://doi.org/10.1016/j.neurobiolaging.2014.05.005

Alquezar, C., Arya, S., Kao, A.W., 2021. Tau Post-translational Modifications: Dynamic Transformers of Tau Function, Degradation, and Aggregation. Front. Neurol. 11, 595532. https://doi.org/10.3389/fneur.2020.595532

Alrashidi, H., Eaton, S., Heales, S., 2021. Biochemical characterization of proliferative and differentiated SH-SY5Y cell line as a model for Parkinson's disease. Neurochem Int 145, 105009. https://doi.org/10.1016/j.neuint.2021.105009

Annadurai, N., Hrubý, J., Kubíčková, A., Malina, L., Hajdúch, M., Das, V., 2023. Time- and dose-dependent seeding tendency of exogenous tau R2 and R3 aggregates in cells. Biochem Biophys Res Commun 653, 102–105. https://doi.org/10.1016/j.bbrc.2023.02.057

Annadurai, N., Malina, L., Malohlava, J., Hajdúch, M., Das, V., 2022a. Tau R2 and R3 are essential regions for tau aggregation, seeding and propagation. Biochimie 200, 79–86. https://doi.org/10.1016/j.biochi.2022.05.013

Annadurai, N., Malina, L., Salmona, M., Diomede, L., Bastone, A., Cagnotto, A., Romeo, M., Šrejber, M., Berka, K., Otyepka, M., Hajdúch, M., Das, V., 2022b. Antitumour drugs targeting tau R3 VQIVYK and Cys322 prevent seeding of endogenous tau aggregates by exogenous seeds. The FEBS Journal 289, 1929–1949. https://doi.org/10.1111/febs.16270

Batenburg, K.L., Sestito, C., Cornelissen-Steijger, P., van Weering, J.R.T., Price, L.S., Heine, V.M., Scheper, W., 2023. A 3D human co-culture to model neuron-astrocyte interactions in tauopathies. Biol Proced Online 25, 4. https://doi.org/10.1186/s12575-023-00194-2

Beevers, J.E., Lai, M.C., Collins, E., Booth, H.D.E., Zambon, F., Parkkinen, L., Vowles, J., Cowley, S.A., Wade-Martins, R., Caffrey, T.M., 2017. MAPT Genetic Variation and Neuronal Maturity Alter Isoform Expression Affecting Axonal Transport in iPSC-Derived Dopamine Neurons. Stem Cell Reports 9, 587–599. https://doi.org/10.1016/j.stemcr.2017.06.005

Bell, M., Bachmann, S., Klimek, J., Langerscheidt, F., Zempel, H., 2021. Axonal TAU Sorting Requires the C-terminus of TAU but is Independent of ANKG and TRIM46 Enrichment at the AIS. Neuroscience 461, 155–171. https://doi.org/10.1016/j.neuroscience.2021.01.041

Bell, M., Zempel, H., 2022. SH-SY5Y-derived neurons: a human neuronal model system for investigating TAU sorting and neuronal subtype-specific TAU vulnerability. Rev Neurosci 33, 1–15. https://doi.org/10.1515/revneuro-2020-0152

Biswas, S., Kalil, K., 2018. The Microtubule-Associated Protein Tau Mediates the Organization of Microtubules and Their Dynamic Exploration of Actin-Rich Lamellipodia and Filopodia of Cortical Growth Cones. J. Neurosci. 38, 291–307. https://doi.org/10.1523/JNEUROSCI.2281-17.2017

Biundo, F., Del Prete, D., Zhang, H., Arancio, O., D'Adamio, L., 2018. A role for tau in learning, memory and synaptic plasticity. Sci Rep 8, 3184. https://doi.org/10.1038/s41598-018-21596-3

Brodeur, G.M., 2018. Spontaneous regression of neuroblastoma. Cell Tissue Res 372, 277–286. https://doi.org/10.1007/s00441-017-2761-2

Brunden, K.R., Trojanowski, J.Q., Smith, A.B., Lee, V.M.-Y., Ballatore, C., 2014. Microtubule-stabilizing agents as potential therapeutics for neurodegenerative disease. Bioorg Med Chem 22, 5040–5049. https://doi.org/10.1016/j.bmc.2013.12.046

Caceres, A., Kosik, K.S., 1990. Inhibition of neurite polarity by tau antisense oligonucleotides in primary cerebellar neurons. Nature 343, 461–463. https://doi.org/10.1038/343461a0

Caffrey, T.M., Wade-Martins, R., 2007. Functional MAPT haplotypes: Bridging the gap between genotype and neuropathology. Neurobiology of Disease 27, 1–10. https://doi.org/10.1016/j.nbd.2007.04.006

Chen, T.C., Hinton, D.R., Zidovetzki, R., Hofman, F.M., 1998. Up-regulation of the cAMP/PKA pathway inhibits proliferation, induces differentiation, and leads to apoptosis in malignant gliomas. Lab Invest 78, 165–174.

Chen, Y., Stevens, B., Chang, J., Milbrandt, J., Barres, B.A., Hell, J.W., 2008. NS21: re-defined and modified supplement B27 for neuronal cultures. J Neurosci Methods 171, 239–247. https://doi.org/10.1016/j.jneumeth.2008.03.013

Chu, D., Liu, F., 2019. Pathological Changes of Tau Related to Alzheimer's Disease. ACS Chem Neurosci 10, 931–944. https://doi.org/10.1021/acschemneuro.8b00457

Cruts, M., Theuns, J., Van Broeckhoven, C., 2012. Locus-specific mutation databases for neurodegenerative brain diseases. Hum Mutat 33, 1340–1344. https://doi.org/10.1002/humu.22117

Cruz-Garcia, D., Brouwers, N., Malhotra, V., Curwin, A.J., 2020. Reactive oxygen species triggers unconventional secretion of antioxidants and Acb1. Journal of Cell Biology 219, e201905028. https://doi.org/10.1083/jcb.201905028

Dawson, H.N., Ferreira, A., Eyster, M.V., Ghoshal, N., Binder, L.I., Vitek, M.P., 2001. Inhibition of neuronal maturation in primary hippocampal neurons from tau deficient mice. J Cell Sci 114, 1179–1187. https://doi.org/10.1242/jcs.114.6.1179

de la Fuente, C., Burke, D.G., Eaton, S., Heales, S.J.R., 2017. Inhibition of neuronal mitochondrial complex I or lysosomal glucocerebrosidase is associated with increased dopamine and serotonin turnover. Neurochem Int 109, 94–100. https://doi.org/10.1016/j.neuint.2017.02.013

De La-Rocque, S., Moretto, E., Butnaru, I., Schiavo, G., 2021. Knockin' on heaven's door: Molecular mechanisms of neuronal tau uptake. J Neurochem 156, 563–588. https://doi.org/10.1111/jnc.15144

de Medeiros, L.M., De Bastiani, M.A., Rico, E.P., Schonhofen, P., Pfaffenseller, B., Wollenhaupt-Aguiar, B., Grun, L., Barbé-Tuana, F., Zimmer, E.R., Castro, M.A.A., Parsons, R.B., Klamt, F., 2019. Cholinergic Differentiation of Human Neuroblastoma SH-SY5Y Cell Line and Its Potential Use as an In vitro Model for Alzheimer's Disease Studies. Mol Neurobiol 56, 7355–7367. https://doi.org/10.1007/s12035-019-1605-3

Demaegd, K., Schymkowitz, J., Rousseau, F., 2018. Transcellular Spreading of Tau in Tauopathies. Chembiochem 19, 2424–2432. https://doi.org/10.1002/cbic.201800288

Dujardin, S., Commins, C., Lathuiliere, A., Beerepoot, P., Fernandes, A.R., Kamath, T.V., De Los Santos, M.B., Klickstein, N., Corjuc, D.L., Corjuc, B.T., Dooley, P.M., Viode, A., Oakley, D.H., Moore, B.D., Mullin, K., Jean-Gilles, D., Clark, R., Atchison, K., Moore, R., Chibnik, L.B., Tanzi, R.E., Frosch, M.P., Serrano-Pozo, A., Elwood, F., Steen, J.A., Kennedy,

M.E., Hyman, B.T., 2021. Author Correction: Tau molecular diversity contributes to clinical heterogeneity in Alzheimer's disease. Nat Med 27, 356. https://doi.org/10.1038/s41591-021-01251-7

Dwane, S., Durack, E., Kiely, P.A., 2013. Optimising parameters for the differentiation of SH-SY5Y cells to study cell adhesion and cell migration. BMC Res Notes 6, 366. https://doi.org/10.1186/1756-0500-6-366

Elks, M.L., Manganiello, V.C., 1985. A role for soluble cAMP phosphodiesterases in differentiation of 3T3-L1 adipocytes. J Cell Physiol 124, 191–198. https://doi.org/10.1002/jcp.1041240204

Ferrari-Souza, J.P., Ferreira, P.C.L., Bellaver, B., Tissot, C., Wang, Y.-T., Leffa, D.T., Brum, W.S., Benedet, A.L., Ashton, N.J., De Bastiani, M.A., Rocha, A., Therriault, J., Lussier, F.Z., Chamoun, M., Servaes, S., Bezgin, G., Kang, M.S., Stevenson, J., Rahmouni, N., Pallen, V., Poltronetti, N.M., Klunk, W.E., Tudorascu, D.L., Cohen, A.D., Villemagne, V.L., Gauthier, S., Blennow, K., Zetterberg, H., Souza, D.O., Karikari, T.K., Zimmer, E.R., Rosa-Neto, P., Pascoal, T.A., 2022. Astrocyte biomarker signatures of amyloid-β and tau pathologies in Alzheimer's disease. Mol Psychiatry 27, 4781–4789. https://doi.org/10.1038/s41380-022-01716-2

Furman, J.L., Vaquer-Alicea, J., White, C.L., Cairns, N.J., Nelson, P.T., Diamond, M.I., 2017. Widespread tau seeding activity at early Braak stages. Acta Neuropathol 133, 91–100. https://doi.org/10.1007/s00401-016-1644-z

Fuster-Matanzo, A., Hernández, F., Ávila, J., 2018. Tau Spreading Mechanisms; Implications for Dysfunctional Tauopathies. IJMS 19, 645. https://doi.org/10.3390/ijms19030645

Ganne, A., Balasubramaniam, M., Griffin, W.S.T., Shmookler Reis, R.J., Ayyadevara, S., 2022. Glial Fibrillary Acidic Protein: A Biomarker and Drug Target for Alzheimer's Disease. Pharmaceutics 14, 1354. https://doi.org/10.3390/pharmaceutics14071354

Georges, J., Miller, O., Bintener, C., 2020. Estimating the prevalence of dementia in Europe. https://doi.org/10.13140/RG.2.2.16880.81923

Goedert, M., Jakes, R., 1990. Expression of separate isoforms of human tau protein: correlation with the tau pattern in brain and effects on tubulin polymerization. EMBO J 9, 4225–4230. https://doi.org/10.1002/j.1460-2075.1990.tb07870.x

Han, P., Serrano, G., Beach, T.G., Caselli, R.J., Yin, J., Zhuang, N., Shi, J., 2017. A Quantitative Analysis of Brain Soluble Tau and the Tau Secretion Factor. J Neuropathol Exp Neurol 76, 44–51. https://doi.org/10.1093/jnen/nlw105

Harada, A., Oguchi, K., Okabe, S., Kuno, J., Terada, S., Ohshima, T., Sato-Yoshitake, R., Takei, Y., Noda, T., Hirokawa, N., 1994. Altered microtubule organization in small-calibre axons of mice lacking tau protein. Nature 369, 488–491. https://doi.org/10.1038/369488a0

Heinisch, J.J., Brandt, R., 2016. Signaling pathways and posttranslational modifications of tau in Alzheimer's disease: the humanization of yeast cells. MIC 3, 135–146. https://doi.org/10.15698/mic2016.04.489

Holmes, B.B., DeVos, S.L., Kfoury, N., Li, M., Jacks, R., Yanamandra, K., Ouidja, M.O., Brodsky, F.M., Marasa, J., Bagchi, D.P., Kotzbauer, P.T., Miller, T.M., Papy-Garcia, D., Diamond, M.I., 2013. Heparan sulfate proteoglycans mediate internalization and propagation of specific proteopathic seeds. Proc Natl Acad Sci U S A 110, E3138-3147. https://doi.org/10.1073/pnas.1301440110

Joshi, S., Guleria, R., Pan, J., DiPette, D., Singh, U.S., 2006. Retinoic acid receptors and tissue-transglutaminase mediate short-term effect of retinoic acid on migration and invasion of neuroblastoma SH-SY5Y cells. Oncogene 25, 240–247. https://doi.org/10.1038/sj.onc.1209027

Jung, G.-S., Lee, K.-M., Park, J.-K., Choi, S.-K., Jeon, W.B., 2013. Morphogenetic and neuronal characterization of human neuroblastoma multicellular spheroids cultured under undifferentiated and all-trans-retinoic acid-differentiated conditions. BMB Rep 46, 276–281. https://doi.org/10.5483/bmbrep.2013.46.5.196

Kadavath, H., Hofele, R.V., Biernat, J., Kumar, S., Tepper, K., Urlaub, H., Mandelkow, E., Zweckstetter, M., 2015. Tau stabilizes microtubules by binding at the interface between tubulin heterodimers. Proc Natl Acad Sci U S A 112, 7501–7506. https://doi.org/10.1073/pnas.1504081112

Kapałczyńska, M., Kolenda, T., Przybyła, W., Zajączkowska, M., Teresiak, A., Filas, V., Ibbs, M., Bliźniak, R., Łuczewski, Ł., Lamperska, K., 2018. 2D and 3D cell cultures - a comparison of different types of cancer cell cultures. Arch Med Sci 14, 910–919. https://doi.org/10.5114/aoms.2016.63743

Karch, C.M., Kao, A.W., Karydas, A., Onanuga, K., Martinez, R., Argouarch, A., Wang, C., Huang, C., Sohn, P.D., Bowles, K.R., Spina, S., Silva, M.C., Marsh, J.A., Hsu, S., Pugh, D.A., Ghoshal, N., Norton, J., Huang, Y., Lee, S.E., Seeley, W.W., Theofilas, P., Grinberg, L.T., Moreno, F., McIlroy, K., Boeve, B.F., Cairns, N.J., Crary, J.F., Haggarty, S.J., Ichida, J.K., Kosik, K.S., Miller, B.L., Gan, L., Goate, A.M., Temple, S., Tau Consortium Stem Cell Group, 2019. A Comprehensive Resource for Induced Pluripotent Stem Cells from Patients with Primary Tauopathies. Stem Cell Reports 13, 939–955. https://doi.org/10.1016/j.stemcr.2019.09.006

Kent, S.A., Spires-Jones, T.L., Durrant, C.S., 2020. The physiological roles of tau and Aβ: implications for Alzheimer's disease pathology and therapeutics. Acta Neuropathol 140, 417–447. https://doi.org/10.1007/s00401-020-02196-w

Khwanraj, K., Phruksaniyom, C., Madlah, S., Dharmasaroja, P., 2015. Differential Expression of Tyrosine Hydroxylase Protein and Apoptosis-Related Genes in Differentiated and Undifferentiated SH-SY5Y Neuroblastoma Cells Treated with MPP(.). Neurol Res Int 2015, 734703. https://doi.org/10.1155/2015/734703

Kimura, T., Whitcomb, D.J., Jo, J., Regan, P., Piers, T., Heo, S., Brown, C., Hashikawa, T., Murayama, M., Seok, H., Sotiropoulos, I., Kim, E., Collingridge, G.L., Takashima, A., Cho, K., 2014. Microtubule-associated protein tau is essential for long-term depression in the hippocampus. Phil. Trans. R. Soc. B 369, 20130144. https://doi.org/10.1098/rstb.2013.0144

Kovalevich, J., Langford, D., 2013. Considerations for the use of SH-SY5Y neuroblastoma cells in neurobiology. Methods Mol Biol 1078, 9–21. https://doi.org/10.1007/978-1-62703-640-5_2

Kumawat, K., Gosens, R., 2016. WNT-5A: signaling and functions in health and disease. Cell Mol Life Sci 73, 567–587. https://doi.org/10.1007/s00018-015-2076-y

Liu, L., Ding, L., Rovere, M., Wolfe, M.S., Selkoe, D.J., 2019. A cellular complex of BACE1 and γ-secretase sequentially generates Aβ from its full-length precursor. Journal of Cell Biology 218, 644–663. https://doi.org/10.1083/jcb.201806205

Martin, E.-R., Gandawijaya, J., Oguro-Ando, A., 2022. A novel method for generating glutamatergic SH-SY5Y neuron-like cells utilizing B-27 supplement. Front Pharmacol 13, 943627. https://doi.org/10.3389/fphar.2022.943627

Merezhko, M., Brunello, C.A., Yan, X., Vihinen, H., Jokitalo, E., Uronen, R.-L., Huttunen, H.J., 2018. Secretion of Tau via an Unconventional Non-vesicular Mechanism. Cell Rep 25, 2027-2035.e4. https://doi.org/10.1016/j.celrep.2018.10.078

Merrill, R.A., Ahrens, J.M., Kaiser, M.E., Federhart, K.S., Poon, V.Y., Clagett-Dame, M., 2004. All-trans retinoic acid-responsive genes identified in the human SH-SY5Y neuroblastoma cell line and their regulated expression in the nervous system of early embryos. Biol Chem 385, 605–614. https://doi.org/10.1515/BC.2004.075

Mohamed, N.-V., Plouffe, V., Rémillard-Labrosse, G., Planel, E., Leclerc, N., 2014. Starvation and inhibition of lysosomal function increased tau secretion by primary cortical neurons. Sci Rep 4, 5715. https://doi.org/10.1038/srep05715

Monterey, M.D., Wei, H., Wu, X., Wu, J.Q., 2021. The Many Faces of Astrocytes in Alzheimer's Disease. Front Neurol 12, 619626. https://doi.org/10.3389/fneur.2021.619626

Nagpal, I., Wei, L.-N., 2019. All-trans Retinoic Acid as a Versatile Cytosolic Signal Modulator Mediated by CRABP1. Int J Mol Sci 20, 3610. https://doi.org/10.3390/ijms20153610

Neve, R.L., Harris, P., Kosik, K.S., Kurnit, D.M., Donlon, T.A., 1986. Identification of cDNA clones for the human microtubule-associated protein tau and chromosomal localization of the genes for tau and microtubule-associated protein 2. Brain Res 387, 271–280. https://doi.org/10.1016/0169-328x(86)90033-1

Pavlou, M.A.S., Grandbarbe, L., Buckley, N.J., Niclou, S.P., Michelucci, A., 2019. Transcriptional and epigenetic mechanisms underlying astrocyte identity. Prog Neurobiol 174, 36–52. https://doi.org/10.1016/j.pneurobio.2018.12.007

Pernègre, C., Duquette, A., Leclerc, N., 2019. Tau Secretion: Good and Bad for Neurons. Front Neurosci 13, 649. https://doi.org/10.3389/fnins.2019.00649

Presgraves, S.P., Ahmed, T., Borwege, S., Joyce, J.N., 2003. Terminally differentiated SH-SY5Y cells provide a model system for studying neuroprotective effects of dopamine agonists. neurotox res 5, 579–598. https://doi.org/10.1007/BF03033178

Qiang, L., Sun, X., Austin, T.O., Muralidharan, H., Jean, D.C., Liu, M., Yu, W., Baas, P.W., 2018. Tau Does Not Stabilize Axonal Microtubules but Rather Enables Them to Have Long Labile Domains. Curr Biol 28, 2181-2189.e4. https://doi.org/10.1016/j.cub.2018.05.045

Qiao, J., Paul, P., Lee, S., Qiao, L., Josifi, E., Tiao, J.R., Chung, D.H., 2012. PI3K/AKT and ERK regulate retinoic acid-induced neuroblastoma cellular differentiation. Biochem Biophys Res Commun 424, 421–426. https://doi.org/10.1016/j.bbrc.2012.06.125

Roda, A.R., Serra-Mir, G., Montoliu-Gaya, L., Tiessler, L., Villegas, S., 2022. Amyloid-beta peptide and tau protein crosstalk in Alzheimer's disease. Neural Regen Res 17, 1666–1674. https://doi.org/10.4103/1673-5374.332127

Ruiz-Gabarre, D., Carnero-Espejo, A., Ávila, J., García-Escudero, V., 2022. What's in a Gene? The Outstanding Diversity of MAPT. Cells 11, 840. https://doi.org/10.3390/cells11050840

Saman, Sudad, Kim, W., Raya, M., Visnick, Y., Miro, S., Saman, Sarmad, Jackson, B., McKee, A.C., Alvarez, V.E., Lee, N.C.Y., Hall, G.F., 2012. Exosome-associated tau is secreted in tauopathy models and is selectively phosphorylated in cerebrospinal fluid in early Alzheimer disease. J Biol Chem 287, 3842–3849. https://doi.org/10.1074/jbc.M111.277061

Sapir, T., Frotscher, M., Levy, T., Mandelkow, E.-M., Reiner, O., 2012. Tau's role in the developing brain: implications for intellectual disability. Human Molecular Genetics 21, 1681–1692. https://doi.org/10.1093/hmg/ddr603

Sasaki, T., Yamazaki, K., Yamori, T., Endo, T., 2002. Inhibition of proliferation and induction of differentiation of glioma cells with Datura stramonium agglutinin. Br J Cancer 87, 918–923. https://doi.org/10.1038/sj.bjc.6600550

Sayas, C.L., Ávila, J., 2014. Crosstalk between axonal classical microtubule-associated proteins and end binding proteins during axon extension: possible implications in neurodegeneration. J Alzheimers Dis 40 Suppl 1, S17-22. https://doi.org/10.3233/JAD-132315

Seidel, D., Krinke, D., Jahnke, H.-G., Hirche, A., Kloß, D., Mack, T.G.A., Striggow, F., Robitzki, A., 2012. Induced Tauopathy in a Novel 3D-Culture Model Mediates Neurodegenerative Processes: A Real-Time Study on Biochips. PLoS ONE 7, e49150. https://doi.org/10.1371/journal.pone.0049150

Strang, K.H., Croft, C.L., Sorrentino, Z.A., Chakrabarty, P., Golde, T.E., Giasson, B.I., 2018. Distinct differences in prion-like seeding and aggregation between Tau protein variants provide mechanistic insights into tauopathies. J Biol Chem 293, 2408–2421. https://doi.org/10.1074/jbc.M117.815357

Strother, L., Miles, G.B., Holiday, A.R., Cheng, Y., Doherty, G.H., 2021. Long-term culture of SH-SY5Y neuroblastoma cells in the absence of neurotrophins: A novel model of neuronal ageing. Journal of Neuroscience Methods 362, 109301. https://doi.org/10.1016/j.jneumeth.2021.109301

Takeda, S., Wegmann, S., Cho, H., DeVos, S.L., Commins, C., Roe, A.D., Nicholls, S.B., Carlson, G.A., Pitstick, R., Nobuhara, C.K., Costantino, I., Frosch, M.P., Müller, D.J., Irimia, D., Hyman, B.T., 2015. Neuronal uptake and propagation of a rare phosphorylated high-molecular-weight tau derived from Alzheimer's disease brain. Nat Commun 6, 8490. https://doi.org/10.1038/ncomms9490

Tio, M., Tan, K.H., Lee, W., Wang, T.T., Udolph, G., 2010. Roles of db-cAMP, IBMX and RA in aspects of neural differentiation of cord blood derived mesenchymal-like stem cells. PLoS One 5, e9398. https://doi.org/10.1371/journal.pone.0009398

Velazquez, R., Ferreira, E., Tran, A., Turner, E.C., Belfiore, R., Branca, C., Oddo, S., 2018. Acute tau knockdown in the hippocampus of adult mice causes learning and memory deficits. Aging Cell 17, e12775. https://doi.org/10.1111/acel.12775

Wang, H., Imai, Y., Kataoka, A., Takahashi, R., 2007. Cell Type-Specific Upregulation of Parkin in Response to ER Stress. Antioxidants & Redox Signaling 9, 533–542. https://doi.org/10.1089/ars.2006.1522

Wang, Y., Balaji, V., Kaniyappan, S., Krüger, L., Irsen, S., Tepper, K., Chandupatla, R., Maetzler, W., Schneider, A., Mandelkow, E., Mandelkow, E.-M., 2017. The release and trans-synaptic transmission of Tau via exosomes. Mol Neurodegeneration 12, 5. https://doi.org/10.1186/s13024-016-0143-y

Welch, W.C., Morrison, R.S., Gross, J.L., Gollin, S.M., Kitson, R.B., Goldfarb, R.H., Giuliano, K.A., Bradley, M.K., Kornblith, P.L., 1995. Morphologic, immunologic, biochemical, and cytogenetic characteristics of the human glioblastoma-derived cell line, SNB-19. In Vitro Cell Dev Biol Anim 31, 610–616. https://doi.org/10.1007/BF02634314

Xicoy, H., Wieringa, B., Martens, G.J.M., 2017. The SH-SY5Y cell line in Parkinson's disease research: a systematic review. Mol Neurodegeneration 12, 10. https://doi.org/10.1186/s13024-017-0149-0

Xie, H., Hu, L., Li, G., 2010. SH-SY5Y human neuroblastoma cell line: in vitro cell model of dopaminergic neurons in Parkinson's disease. Chin Med J (Engl) 123, 1086–1092.

Yu, W., Qiang, L., Solowska, J.M., Karabay, A., Korulu, S., Baas, P.W., 2008. The Microtubule-severing Proteins Spastin and Katanin Participate Differently in the Formation of Axonal Branches. MBoC 19, 1485–1498. https://doi.org/10.1091/mbc.e07-09-0878

Yu, Y., Run, X., Liang, Z., Li, Y., Liu, F., Liu, Y., Iqbal, K., Grundke-Iqbal, I., Gong, C.-X., 2009. Developmental regulation of tau phosphorylation, tau kinases, and tau phosphatases. J Neurochem 108, 1480–1494. https://doi.org/10.1111/j.1471-4159.2009.05882.x

Internet Resources

MUTATIONS/MAPT| Alzforum. (n.d.). Retrieved May 1, 2023, from https://www.alzforum.org/mutations/mapt